Redox Biology 70 (2024) 103041

Contents lists available at ScienceDirect

Redox Biology

journal homepage: www.elsevier.com/locate/redox

Endothelial transferrin receptor 1 contributes to thrombogenesis through cascade ferroptosis

Haotian Ma [a,b], Yongtao Huang [c], Wenrong Tian [a,b], Jincen Liu [a,b], Xinyue Yan [a,b], Lei Ma [a,b], Jianghua Lai [a,b,*]

[a] NHC Key Laboratory of Forensic Science, College of Forensic Medicine, Xi'an Jiaotong University, Xi'an, China
[b] Institute of Forensic Injury, Bio-evidence Sciences Academy, Western China Science and Technology Innovation Harbor, Xi'an Jiaotong University, Xi'an, China
[c] Department of Orthopedics, Ruihua Affiliated Hospital of Soochow University, Suzhou, China

ARTICLE INFO

Keywords:
Transferrin receptor 1
Vascular injury
Ferroptosis
Thrombogenesis
Thrombospondin 1

ABSTRACT

Oxidative stress and iron accumulation-induced ferroptosis occurs in injured vascular cells and can promote thrombogenesis. Transferrin receptor 1 (encoded by the TFRC gene) is an initial element involved in iron transport and ferroptosis and is highly expressed in injured vascular tissues, but its role in thrombosis has not been determined. To explore the potential mechanism and therapeutic effect of TFRC on thrombogenesis, a DVT model of femoral veins (FVs) was established in rats, and weighted correlation network analysis (WGCNA) was used to identify TFRC as a hub protein that is associated with thrombus formation. TFRC was knocked down by adeno-associated virus (AAV) or lentivirus transduction in FVs or human umbilical vein endothelial cells (HUVECs), respectively. Thrombus characteristics and ferroptosis biomarkers were evaluated. Colocalization analysis, molecular docking and coimmunoprecipitation (co-IP) were used to evaluate protein interactions. Tissue-specific TFRC knockdown alleviated iron overload and redox stress, thereby preventing ferroptosis in injured FVs. Loss of TFRC in injured veins could alleviate thrombogenesis, reduce thrombus size and attenuate hypercoagulability. The protein level of thrombospondin-1 (THBS1) was increased in DVT tissues, and silencing TFRC decreased the protein level of THBS1. In vitro experiments further showed that TFRC and THBS1 were sensitive to erastin-induced ferroptosis and that TFRC knockdown reversed this effect. TFRC can interact with THBS1 in the domain spanning from TSR1-2 to TSR1-3 of THBS1. Amino acid sites, including GLN320 of TFRC and ASP502 of THBS1, could be potential pharmacological targets. Erastin induced ferroptosis affected extracellular THBS1 levels and weakened the interaction between TFRC and THBS1 both in vivo and in vitro, and promoted the interaction between THBS1 and CD47. This study revealed a linked relationship between venous ferroptosis and coagulation cascades. Controlling TFRC and ferroptosis in endothelial cells can be an efficient approach for preventing and treating thrombogenesis.

1. Introduction

In clinical medical practice, trauma to deep venous tissues can readily result in deep vein thrombus (DVT), necessitating advanced pharmacological management strategies. Discovering potential mechanism of vascular injury and thrombogenesis is important to the treatment and drug intervention of DVT. Traumatic injury is a major cause of tissue redox stress, hypoxia, and ischemia reperfusion, factors above can induce cell death. Vascular cells in thrombosis can undergo various types of cell death, previous studies have shown that high iron levels are associated with thrombosis, suggesting the important role of iron homeostasis in thrombotic events [1]. Ferroptosis is induced by the overload of iron and closely related to vascular injury [2]. Iron levels in mechanical injured vascular tissue can be significantly increased, as proven in previous studies [3]. Excess free divalent iron can exacerbate oxidative stress. Researchers created an iron load model in mice after long-term administration of dextran iron and found that iron accumulation significantly accelerated thrombosis after vascular injury and increased vascular oxidative stress [4]. The formation of DVT accompanied by a reactive oxygen species (ROS) burst has been extensively reported in previous studies [5–8]. ROS further react with polyunsaturated fatty acids on the cell membrane, causing ferroptosis [9]. Our previous work showed that ferroptosis plays a positive role in the

* Corresponding author. College of Forensic Medicine, Xi'an Jiaotong University, No. 76, Yanta West Road, Xi'an, 710061, Shaanxi Province, China.
E-mail address: laijh1011@mail.xjtu.edu.cn (J. Lai).

https://doi.org/10.1016/j.redox.2024.103041
Received 24 December 2023; Received in revised form 8 January 2024; Accepted 11 January 2024
Available online 12 January 2024

Abbreviation

AAV	Adeno-Associated Virus
CD36	Collagen type I receptor
CD47	Integrin-associated protein
co-IP	Coimmunoprecipitation
COX2	Cyclooxygenase 2
CSA	Cross-Sectional Area
DFOM	Deferoxamine Mesylate
DHE	Dihydroethidium
DVT	Deep Vein Thrombus
FVs	Femoral Veins
GPX4	Glutathione peroxidase 4
GSH	Glutathione
GSSG	Oxidized glutathione
H2DCFDA	2′,7′-Dichlorodihydrofluorescein diacetate
HUVECs	Human Umbilical Vein Endothelial Cells
ROS	Reactive Oxygen Species
MDA	Malondialdehyde
MMP	Mitochondrial Membrane Potential
PI	Propidium Iodide
PPI	Protein–Protein Interaction
TF	Tissue Factor
TFRC	Transferrin receptor 1
THBS1	Thrombospondin 1
TSA	Tyramide Signal Amplification
vWF	von Willebrand Factor
WGCNA	Weighted Correlation Network Analysis

formation of thrombosis induced by vascular mechanical injury, and the use of ferroptosis inhibitors can reverse this process [3]. Taken together, these findings suggest that mediating iron homeostasis in injured vessels may be an effective treatment strategy for thrombosis.

In cells, transferrin receptor 1 (TFRC) regulates iron transport, storage, and other processes [10]. TFRC is not only an initial marker and promoter of ferroptosis but is also a diagnostic biomarker of DVT [11]. Several studies have shown that TFRC is highly expressed in DVT patients and animal models [3,11]. Furthermore, in early work, ferroptosis which was characterized by high TFRC expression, was identified through previous experiments [12,13]. What could TFRC regulate in thrombosis? There were few clues left in previous studies. Fortunately, a protein–protein interaction network was built based on our previous proteomics analysis. Thrombospondin 1 (THBS1), a well-known adhesive glycoprotein that is involved in thrombosis, was identified as an interactive partner with TFRC [3,14]. These two proteins showed high and sustained co-expression in injured venous tissues.

In this study, we examined the role of TFRC in DVT and explored the potential mechanism in vivo and in vitro. This is the first study on the effect of TFRC on thrombosis. We formulated the following hypotheses: (i) TFRC is highly expressed after vascular trauma and induces iron accumulation, causing ferroptosis; (ii) knocking down TFRC can ameliorate ferroptosis and thrombogenesis in rats and rescue erastin-induced ferroptosis in human umbilical vein endothelial cells (HUVECs); and (iii) an interaction exists between TFRC and THBS1, and controlling the expression of TFRC can affect the expression of THBS1. Our verification of these hypotheses provides experimental evidence and offers new insights into the pathophysiology and pharmacological intervention of thrombosis.

2. Materials and methods

2.1. Animals and experimental setup

Eighty male Sprague Dawley rats (specific pathogen-free, average weight of 110 ± 22 g) were purchased from the Experimental Animal Center of Xi'an Jiaotong University. The rats were housed in individually ventilated cages under standard conditions. All the experimental procedures were approved by the Institutional Animal Care and Use Committee of Xi'an Jiaotong University. All the experiments were performed according to the UK Animals (Scientific Procedures) Act. All the rats were allowed to adapt to the environment for two weeks. The animal experiments included three parts (Fig. S1A).

Part 1: Twenty-four rats were divided into two groups: the sham and DVT groups (n = 12 for each group). Rats in the sham groups underwent only a sham operation, and rats in the DVT groups underwent DVT model establishment.

Sham operation procedure: Anesthesia was induced and maintained via inhalation of 4 % and 1 % isoflurane. The femoral arteries, veins and nerves were separated via blunt dissection after the inner skin of the bilateral groin was incised. Both bilateral femoral veins were separated. The continuous suture method was used to close the incision.

The DVT model was established according to a previously described method with simple modifications (Fig. 1A) [3,15]. Briefly, anesthesia was induced and maintained via inhalation of 4 % and 1 % isoflurane. The femoral arteries, veins and nerves were separated via blunt dissection after the inner skin of the bilateral groin was incised. The FVs were crushed and blocked by fastening one tooth buckle of the 12.5 mm mosquito clamp at three positions for 3 s to cause venous injury. The model was established on both bilateral FVs. Severely clamped-crushed samples (in which both the media and adventitia were crushed) exhibited signs of hemorrhage or vein rupture and were excluded from the comparative analyses. For the rats that underwent DVT surgery, the injured limb was immobilized with a plaster bandage for 24 h.

After 24 h, the rats were sacrificed after isoflurane anesthetization, and FV samples were collected for ROS assessment, Perl staining and immunofluorescence colocalization.

Part 2: Eight rats were divided into two groups: the DVT and DVT + liproxstatin-1 (ferroptosis inhibitor) groups (n = 4 for each group). Before the 2-h model establishment operation, rats in the DVT group were administered DMSO-saline solution (10 %, 10 mg/kg BW) via intraperitoneal injection, and rats in the DVT + liproxstatin-1 group were given liproxstatin-1-DMSO-saline solution (MedChemExpress, USA; 10 mg/kg BW). After the model was established, samples were collected from the DVT and DVT + Liproxstatin-1 groups and subjected to co-IP.

In Part 3, forty-eight rats were randomly divided into four groups (n = 12): the scramble, scramble-DVT model (scramble + DVT), shRNA-TFRC (shTFRC) and shRNA-TFRC-DVT (shTFRC + DVT) groups. The animals were subsequently prepared for AAV injection (the detailed methods are described in Section 2.2.).

2.2. AAV injection

A shRNA targeting TFRC was synthesized by Brainvta., Ltd. (Wuhan, China), and the sequence that was used for interference was as follows: GCACTAAACTAGATACCTATG. The vector structure is shown in Fig. S1B. Femoral vein injection of rAAV2/9-U6-shRNA (scramble)-CMV-mCherry-SV40 pA (3.32 E+11 μg/ml per rat) was administered to the rats in the scramble and scramble-DVT groups. The scramble shRNA AAV vector included a scramble shRNA expression box and an mCherry expression box. These expression boxes can be packaged into viral particles and transduced into cells. The scrambled virus was used as a negative control for RNA interference (RNAi) experiments. Before the AAV injection, 3-0 silk was passed under the FV, gently blocking the blood supply. The blood supply was restored until 20 min after AAV

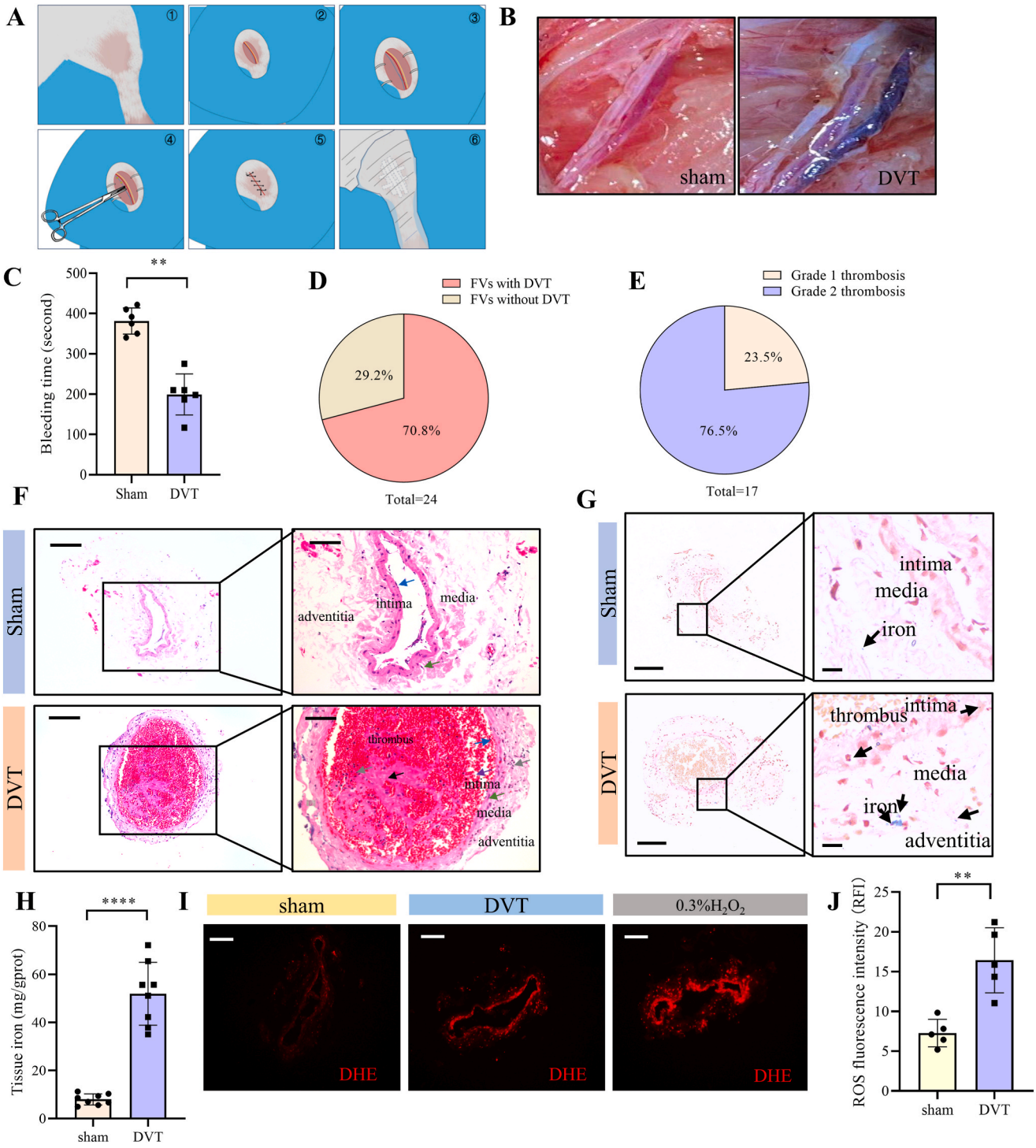

Fig. 1. ROS bursts and iron accumulation in injured femoral veins. (A) DVT establishment procedure, including skin preparation, surgical field exposure, vein, artery and nerve separation, clamp damage, gypsum immobilization and other steps. (B) Gross observation of the femoral veins. (C) Bleeding time of the tail vein (n = 6). The values are expressed as the mean ± SD of replicates. "**" ($P < 0.01$) indicates a significant difference according to the Mann–Whitney *U* test. (D) Thrombosis rate. (E) Proportion of Grade 1 and Grade 2 thrombi. (E) Tissue pathological changes (n = 3); all the tissue samples were cross-sectioned, and the scale bar indicates 100 and 50 μm at low and high magnification, respectively. Endothelial cells (shown by the blue arrow), red blood cells (purple arrow), platelet trabeculae (black arrow), vascular smooth muscle cells (green arrow) and inflammatory cells (gray arrow) are labeled. (F) Perls staining (n = 3) shows the iron contents in vascular tissues (black arrows). The scale bar in the Perls staining images is 100 and 10 μm at low and high magnification, respectively. All the samples were cross-sectioned. (G) Quantitative measurement of tissue iron concentrations; n = 8. Values are expressed as the mean ± SD of replicates, and "****" ($P < 0.0001$) indicates a significant difference according to the unpaired *t*-test. (I) DHE fluorescence was used to detect ROS; n = 3. All the samples were cross-sectioned. The scale bar indicates 100 μm. Treatment with 0.3 % H_2O_2 was used as a positive control. (J) Quantitative measurement of tissue ROS levels; n = 5. The values are expressed as the mean ± SD of replicates, and statistical analysis was performed with the Mann–Whitney *U* test. "**" ($P < 0.01$) indicates a significant difference. (For interpretation of the references to color in this figure legend, the reader is referred to the Web version of this article.)

injection. AAV2/9 was injected into both bilateral femoral veins. All the treatments were administered three weeks before model establishment. After three weeks, the injected AAV was fully expressed.

Rats in the shTFRC and shTFRC + DVT groups were given rAAV2/9-U6-shRNA (TFRC)-CMV-mCherry-SV40 pA (3.32 E+11 μg/ml per rat) by femoral vein injection. Before the AAV injection, 3-0 silk was passed under the FV, gently blocking the blood supply. The blood supply was restored until 20 min after AAV injection. AAV2/9 was injected into both bilateral femoral veins. All the treatments were administered three weeks before model establishment. After three weeks, the injected AAV was fully expressed. Virus injection and DVT model establishment surgery were performed by different researchers. The researcher who established the DVT model was blinded to the details of the AAV information; they only knew that there were sham and DVT groups. Rats in the scramble and shTFRC groups underwent only a sham operation (as described in Method 2.1), and rats in the DVT groups underwent a model establishment operation. After surgery, the incision was closed via the continuous suture method. The injured limb was immobilized with a plaster bandage for 24 h. After 24 h, the rats were sacrificed after isoflurane anesthetization, and FV samples were collected for subsequent analysis.

2.3. Cells and experimental setup

HUVECs were purchased from the Shanghai Cell Bank of the Chinese Academy of Sciences and cultured in Dulbecco's modified Eagle's medium supplemented with 10 % fetal bovine serum and 1 % (v/v) penicillin/streptomycin in a 37 °C incubator with a humidified atmosphere of 5 % CO_2. The passage number of the cell lines was approximately F3∼F5.

A shRNA targeting TFRC was synthesized by Tsingke Biotechnology Co., Ltd. (Beijing, China), and the sequence that was used for interference was as follows: GCTGGTCAGTTCGTGATTAAA. The vector structure is shown in Fig. S4C. HUVECs were transfected with TFRC shRNA or negative control shRNA using polybrene reagent. The cells were transduced with lentivirus (multiplicity of infection = 100). After three days, stable clones expressing the shRNA were selected via puromycin dihydrochloride (MedChemExpress, China). The medium was replaced with new puromycin-supplemented medium every 2–3 days until resistant colonies were selected. The resistant colonies were expanded, and GFP fluorescence and Western blotting analyses were performed to evaluate stable shRNA transduction and knockdown efficiency. Normal cells and transinfected cells were treated with DMSO (vehicle reagent), erastin (ferroptosis agonist, HY-15763; MedChemExpress), or deferoxamine mesylate (iron chelator, DFOM; HY-B0988; MedChemExpress) for 24 h.

2.4. Thrombosis classification and sample collection

All the rats were anesthetized 24 h after DVT surgery. Two researchers who were blinded to the experimental setup performed the bleeding test and thrombosis classification. A scalpel was used to transect the tip of the tail at 5 mm, and the time from bleeding to hemostasis was recorded. Then, the length of the thrombus was measured. The femoral vein is too thin, so a needle (29 G or 30 G) cannot be used to assist in the determination of the occlusion area. Thus, the grading of the tumors was analyzed through a Vernier caliper to orthoptically measure the diameter of the vein and the thrombus under a dissecting microscope (Leica, Germany). Thrombosis was classified into two grades [3,16]. A thrombus with an DVT obstruction area that accounted for less than 50 % of the cross-sectional area (CSA) of the FV was considered Grade 1; a thrombus with an DVT obstruction area that accounted for more than 50 % of the CSA of the FV was classified as Grade 2. The vacuum blood drawing technique was used to collect blood samples from the inferior vena cava.

To avoid bias, all the injured venous tissues (except for severe clamp-crushed samples, as described in paragraph 2.1), regardless of whether thrombosis had formed or the grade of the thrombus, were collected by researchers who performed thrombosis grading. The FV tissues were carefully washed with normal saline, and only the venous tissues were collected and stored in specially labeled EP tubes for further analysis. When Western blotting and biochemical tests were conducted, the operators were blinded to the thrombus grade. For HE staining, tissues were immersed in 4 % paraformaldehyde. Rats were sacrificed after isoflurane anesthetization. The FV samples were dehydrated through gradient ethanol after fixation. FVs were embedded in paraffin wax blocks after vitrification, and five-micron-thick sections were prepared. The sections were stained with HE reagents after dewaxing in xylene and rehydrating. Images of the tissues were captured under a microscope (Leica, Germany).

2.5. WGCNA and pathway enrichment analysis of label-free quantitative proteomics data from normal and DVT FVs

The WGCNA package (version 1.71) of the R language was used to construct a co-expression network based on our previous label-free quantitative proteomics data from venous samples in the sham and DVT groups. Our sequencing data were deposited in the ProteomeXchange Consortium database (http://proteomecentral.proteomexchange.org) with the identifier PXD032343. The setting parameters were as follows: soft power (β), 18 (Fig. S1D); minModuleSize, 25; deepSplit, 2; and outlier sample detection threshold, −2.5. Modules with highly correlated proteins were aggregated into the same color region, and Pearson correlation analysis and significance analysis were used to calculate the proteins of the module and thrombus formation in the sample. Hub proteins were automatically selected through a protein–protein interaction (PPI) network based on WGCNA. Information on proteins that may interact with TFRC in endothelial cells was downloaded from the PROPER dataset. All the PPI networks were optimized with Cytoscape software (3.9.1). An expression heatmap of several iron homeostasis-related proteins was constructed based on our public dataset.

Kyoto Encyclopedia of Genes and Genomes (KEGG) and Gene Ontology (GO) Analyses. GO and KEGG enrichment analyses of proteins that were upregulated in the DVT/sham group were performed with KOBAS 3.0 (http://bioinfo.org/kobas) and R software (3.6.1). GO and KEGG pathway enrichment analysis results were considered statistically significant when $P < 0.05$.

2.6. Evaluation of HUVEC viability

CCK8 assays and propidium iodide (PI) staining were used to determine the viability of the HUVECs. HUVECs were seeded in 94-well plates. Cells were treated with DMSO, erastin or DFOM and cultured for at least 24 h. CCK8 reagent was added, and the optical density (OD) of each well was measured at 450 nm with a microplate reader (Thermo Fisher Scientific). The percentage of viable cells was calculated according to the OD values. PI was chosen for staining cell slides due to its ability to detect dead cells. DAPI was used to label the cell nucleus. The sections were observed under a fluorescence microscope, and the number of positive cells was counted by using the ImageJ tool (ImageJ, 1.48; National Institutes of Health, USA).

2.7. Measurement of ROS levels

Tissue ROS measurement was performed as previously described [17]. Fresh venous tissues were washed with 1× PBS and mounted in OCT embedding compound to prepare frozen sections (the tissues were not fixed). Frozen sections (10 μm) were cut using a freezing microtome (Leica, Germany). An H2DCFDA kit (MedChemExpress, China) or DHE probe (MedChemExpress, China) was used to determine the ROS levels in the FV tissues. For rats transduced with AAV2/9, we chose the probe H2DCFDA (10 μM) to measure the ROS levels to avoid interference of

red mCherry signals. Then, 10 μM DHE-PBS or 10 μM H2DCFDA-PBS was added to the frozen tissue sections, which were incubated at 37 °C in the dark for 30 min and washed three times with 1 × PBS. Treatment with 0.3 % H_2O_2 (10 min) was used as a positive control. The sections were observed under a fluorescence microscope (excitation wavelength: DHE 488 nm; H2DCFDA 485 nm; Leica, Germany). The relative fluorescence intensity (RFI) of the ROS in tissues was quantified by ImageJ. Sections were stained with DAPI before representative images were captured with a fluorescence microscope.

For intracellular ROS detection, ROS levels were measured following the protocol of an H2DCFDA kit (Solarbio, China) or DHE probe (MedChemExpress, China). HUVECs were cultured in 6-well plates and then exposed to an erastin suspension or erastin + DFOM treatment for 24 h. Afterward, the cells were enzymatically digested with trypsin and collected and then incubated in 10 μM H2DCFDA-PBS for 20 min at 37 °C in the dark. Treatment with 0.3 % H_2O_2 (10 min) was used as a positive control. After incubation, the cells were washed with PBS to remove the probes. For cells transduced with lentivirus, to avoid GFP interference, we used 10 μM DHE probe to measure the intracellular ROS concentration, and the procedure was the same as that for the H2DCFDA method.

Cell slides were prepared and subsequently incubated with a 10 μM H2DCFDA probe solution for 25 min at 37 °C in the dark. The sections were observed under a fluorescence microscope (excitation wavelength 485 nm; Leica, Germany). Treatment with 0.3 % H_2O_2 (10 min) was used as a positive control. Sections were stained with DAPI before representative images were captured with a fluorescence microscope.

Carboxy-DCFDA was used as a control [18]. When the H2DCFDA method was used, tissue sections and HUVECs were labeled with both H2DCFDA and carboxy-DCFDA (insensitive to oxidation; C369, Invitrogen). The concentration and staining procedure of carboxy-DCFDA was the same as those of H2DCFDA. The ratio of the fluorescence intensities of H2DCFDA and DCFDA (H2DCFDA/DCFDA) was used to normalize cell number, influx, efflux and enzymatic cleavage based on previous methods [19].

2.8. Measurement of iron, malondialdehyde (MDA), MMP, GSSG and GSH levels in plasma, tissues and HUVECs

For quantitative index assessments, tissue or cell samples were mixed with saline (1:9) and ultrasonically disrupted. Blood and tissue homogenate supernatants were collected after centrifugation. GSH fluorescence was detected by using a monochlorobimane probe (MedChemExpress, China), and the fluorescence intensity was measured via fluorescence microscopy at 470 nm. MDA, GSH and GSSG detection kits (Jiancheng, China) were used to measure the relative levels of these indices. Briefly, GSH and GSSG levels were measured by reacting with dithio-dinitrobenzoic acid (DTNB) to form compounds that can be detected via colorimetric measurements at 405 nm. The GSH/GSSG ratio was used to evaluate the GSH balance during oxidation. The FV tissues were homogenized, mixed with MDA working reagent and boiled at 100 °C for 15 min, after which the absorbance was measured at 532 nM.

Iron levels were determined on cell slides and in dissociated FVs with a Perls stain (can stain Fe^{3+} ions) kit (Solarbio, China), and liver, heart and inferior vena cava sections were also stained with Perls. Images of each sample were observed and captured under a microscope (Leica, Germany). Quantification of tissue and serum iron (total iron) levels was performed by using a tissue/serum total iron detection kit (Jiancheng, China). Ferryl in tissues or serum can be reduced to ferrous iron, which combines with dipyridine to form a pink complex that can be detected at 520 nm.

A mitochondrial membrane potential assay kit with JC-1 (Solarbio, China) was used to measure the mitochondrial membrane potential (MMP) of the FV samples. First, mitochondria were obtained with a mitochondria extraction kit (Solarbio, China). The samples were mixed with JC1 working solution and imaged under a fluorescence microscope. Aggregates and monomers of JC1 were detected at 525 and 490 nm excitation, respectively. Images of each sample were captured, and the number of positive cells was counted by using the ImageJ tool (ImageJ, 1.48; National Institutes of Health, USA).

2.9. Immunofluorescence colocalization based on the tyramide signal amplification (TSA) method

Cell slides and frozen tissue sections after different treatments were prepared as described above. Tissue sections were pretreated by antigen retrieval and spontaneous fluorescence quenching. To inactivate endogenous peroxidase, 3 % H_2O_2 was added to the samples, which were subsequently incubated at room temperature for 25 min. After washing three times, the slides and sections were blocked with 3 % BSA at room temperature for 30 min. Then, the slides and sections were incubated overnight with primary antibodies (rabbit *anti*-TFRC, 13113; Cell Signaling Technology, 1:300; rabbit *anti*-THBS1, ab267388; Abcam, 1:300; mouse anti-CD47, No. 66304-1-Ig, Proteintech, 1:200) at 4 °C. After the sections were washed with primary antibodies, the sections were incubated with the appropriate HRP-labeled secondary antibody at room temperature for 50 min. The fluorescent dye Cy3-tyramide (G1223, Servicebio), FITC-tyramide (G1222, Servicebio) or DyLight™ 405 (Goat anti-Mouse IgG (H + L) secondary antibody, 35501, Invitrogen) was added to the samples and allowed to react at room temperature for 10 min. The slides and sections were placed in a repair box filled with antigen repair solution containing 1 × sodium citrate buffer to remove the combined primary and secondary antibodies by microwave heating. The steps described above were repeated, after which the sections were incubated with secondary antibody and TSA markers, and a microwave was used to remove the primary antibody and secondary antibody. Finally, all the slides and sections were sealed with antifade solution containing DAPI and observed under a fluorescence microscope. The colocalization data were analyzed with "colocalization finder" in ImageJ tools.

2.10. Enzyme-linked immunosorbent assay, western blotting, immunofluorescence and immunohistochemistry

Plasma levels of rat D-dimer and tissue factor (Tf, factor III) were measured with ELISA kits following the manufacturer's instructions (Cat No: BY-JZF0129, BY-ER331101, BY abscience, China). For HUVECs, the medium was removed by centrifugation, and the extracellular levels of THBS1 and vWF were measured by following the procedures of the human THBS1 and vWF ELISA kits (Cat No: KE00249, Proteintech; BY-EH180106, BY Biosciences).

Immunofluorescence staining of tissues was performed as follows. Frozen sections of FV tissues were washed with PBS 3 times for 10 min each. We suggest quenching the autofluorescence of the vascular tissues before the next step. After blocking in 5 % BSA in PBST solution for 30 min, the sections were incubated overnight with primary antibodies (rabbit *anti*-TFRC antibody, 13113; Cell Signaling Technology, 1:200; rabbit *anti*-HIF1α antibody, 14179; Cell Signaling Technology, 1:100; rabbit *anti*-THBS1 antibody, ab267388; Abcam, 1:150; and rabbit anti-CD47 antibody, 1:100; A1199; ABclonal) at 4 °C. Then, the sections were washed three times and incubated with Alexa Fluor 488 (ab150077; Abcam, 1:500) for 2–3 h at room temperature. All the sections were observed under a fluorescence microscope. To analyze cells, first, HUVECs were seeded in 24-well plates containing cell slides and DMEM. After incubation, the cell slides were collected and immersed in 4 % paraformaldehyde for 10 min. The remaining steps were similar to those used for immunofluorescence analysis of tissues. The immunohistochemistry procedure was basically the same as the immunofluorescence procedure; the difference was that the target protein was labeled with DAB, and the cell nucleus was stained with hematoxylin.

The samples were mixed with RIPA buffer, and the proteins were collected by centrifugation and sonication. The membrane proteins were

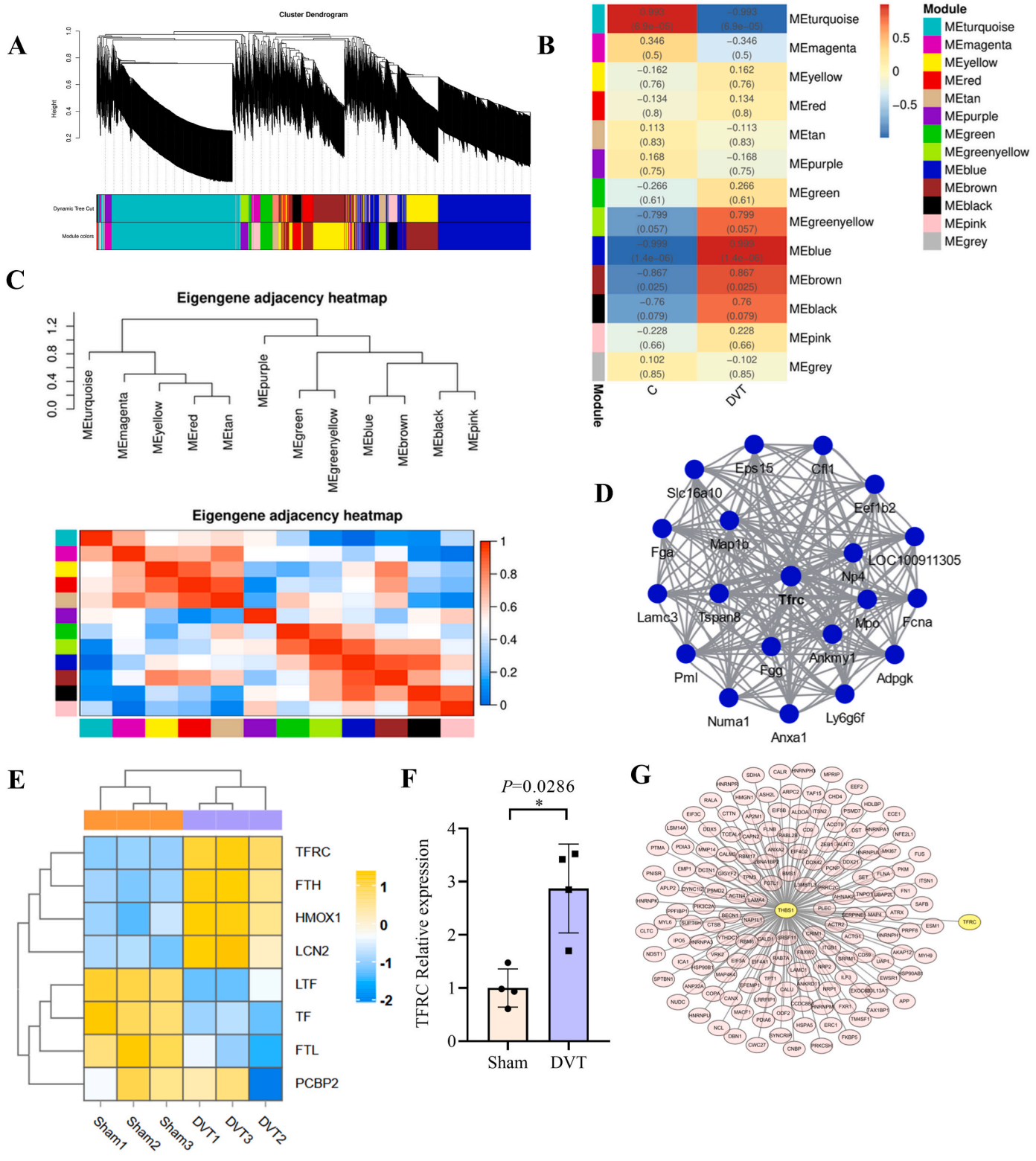

Fig. 2. Identification of TFRC as a hub protein in thrombosis through WGCNA. (A) WGCNA module plot. The initial modules were labeled with dynamic Tree Cut. The module colors represent the final modules. Each branch or each vertical line in the color bars represents one gene. (B) WGCNA module trait correlation plot; each row represents one module. Each column represents one trait attribute. Blue represents a negative correlation, and red represents a positive correlation. (C) WGCNA module correlation plot. (D) Network visualization of WGCNA hub genes. (E) Heatmap of the expression of several iron homeostasis-related proteins in the sham and DVT groups. (F) Protein expression of TFRC; n = 4. The values are expressed as the mean ± SD of replicates. "*" ($P < 0.05$) indicates a significant difference according to the Mann–Whitney *U* test. (G) PPI network based on the PROPER dataset. The nodes corresponding to TRFC and THBS1 are labeled in yellow. (For interpretation of the references to color in this figure legend, the reader is referred to the Web version of this article.)

extracted using a cell membrane protein and cytoplasmic protein extraction kit (P0033, Beyotime). After protein quantification with the BCA method, the extracted protein was separated via SDS–PAGE electrophoresis. The separated proteins were electrotransferred onto polyvinylidene fluoride (PVDF) membranes by the wet transfer method. The membranes were blocked with PBST solution containing 0.1 % Tween 20 and 5 % nonfat dry milk for 2 h. Then, the membranes were incubated overnight with the following primary antibodies: rabbit anti-glutathione peroxidase 4 (GPX4, ab125066, Abcam, 1:2500), rabbit *anti*-cyclooxygenase 2 (COX2, 12282, Cell Signaling Technology, 1:1000), rabbit *anti*-TFRC (13113, Cell Signaling Technology, 1:1000), rabbit *anti*-THBS1 (37879, Cell Signaling Technology, 1:1000), rabbit *anti*-caveolin-1 (A19006, ABclonal, 1:2000) and mouse *anti*-β-actin (3700, Cell Signaling Technology. 1:3000) antibodies. The immunoblots were washed three times with PBST buffer. The membranes were incubated with horseradish peroxidase-conjugated secondary anti-rabbit antibody for 1–2 h at room temperature. Protein bands were detected with an enhanced chemiluminescence (ECL) assay kit after washing the membranes three times.

2.11. Molecular docking and Co-IP

Discovery Studio software was used to process the protein, including the deletion of water molecules, hydrogenation, charge, and extraction of the primary ligand from the structure. Pymol was used to visualize the processed proteins. The Zdock module in Discovery Studio was used to perform protein-to-protein docking. ZDOCK was used for protein docking calculations. ZDOCK is a rigid protein docking algorithm based on the fast Fourier transform correlation technique. The fast Fourier transform correlation technique is used to search for the translational and rotational spaces in protein–protein systems. TFRC was considered the receptor protein, and THBS1 was considered the ligand protein. When the angular step size of the docking sample was set to 6 and the sampling angle was 15°, the prediction results were more accurate because the final sample number included 54000 binding configurations. For such a system, the RMSD cutoff was set to a 10.0 Å cluster radius, the interface cutoff was set to 10.0 Å, and the maximum cluster number was 100. The docking results generated 2000 poses. Then, 16 was selected as the baseline dock score, and key poses were chosen for R-dock docking analysis. The most stable pose was visualized via PyMOL after precise interconnection discovery by R-dock.

Co-IP was performed using a Crosslink Magnetic IP/Co-IP Kit (88805, Thermo Fisher). Cell samples or tissue samples were lysed with IP lysis/wash buffer. A total of 500 μg of lysate was subjected to immunoprecipitation with 2 μg of IgG or 5 μg of primary antibody (normal rabbit IgG, A7058; Beyotime; rabbit *anti*-THBS1 antibody (37879; Cell Signaling Technology)) for 1 h at room temperature. Pierce protein A/G magnetic beads were added for subsequent pull-down and incubated for an additional 1 h at room temperature. The beads were washed with IP lysis/wash buffer, collected via a magnetic frame, and then washed in 1 × lane marker sample buffer to elute immunoprecipitated proteins for further Western blotting analysis. To exclude the effect of the IgG heavy chain, HRP-conjugated mouse anti-rabbit IgG light chain (AS061, 1:10000, ABclonal) was used as the secondary antibody.

2.12. Statistical analysis

The significance of the relationships between categorical variables in the experimental groups was statistically analyzed by Fisher's exact test. For significance tests, the data were subjected to normality and log normality tests, and if they were normally distributed, Tukey's test (T test), one-way ANOVA or two-way ANOVA was performed with Social Sciences (SPSS) software to analyze significant differences; if the data were not normally distributed, choosing the Kruskal-Wally test or Mann–Whitney *U* test. R software (3.6.1), OmicShare tools (https://www.omicshare.com/tools/) and GraphPad Prism 8.3.0 were used to generate the diagrams.

3. Results

3.1. ROS bursts and iron accumulation occur during FV injury the DVT model

After 24 h of DVT induction, as shown in Fig. 1B, there was no significant change in the venous tissues of the sham group, while in the DVT group, black–red ribbons filled the lumen. The tail vein bleeding time showed that the bleeding time of the DVT group was significantly reduced ($n = 6$, $P = 0.022$) by approximately 47.7 % compared with the sham group, indicating the occurrence of hypercoagulability (Fig. 1C). A total of 24 femoral veins were subjected to injury in this study. Postoperative statistics showed that the total success rate of DVT model established by mechanical injury to the femoral veins was approximately 70.8 % (17/24) (Fig. 1D), the average length of the thrombus was approximately 1 cm, the grade 1 thrombus formation rate was 23.5 % (4/17), and the grade 2 thrombus formation rate was approximately 76.5 (13/17) (Fig. 1E). To avoid objective bias, all venous tissues were included in further experiments regardless of thrombosis formation or the grade of the thrombus.

Changes in the tissues were observed by histopathological analysis (Fig. 1F). The pathological description of each group is provided below.

Sham group: No obvious thrombi were evident in the vascular lumen, the structures of the vascular intima and endothelial cells were normal (shown by the blue arrow), and no obvious shedding was observed. No obvious inflammatory cell infiltration was observed in the vascular media or adventitia.

DVT group: Few obvious endothelial cells were observed (blue arrow). Mixed large thrombi, which consisted of red blood cells (purple arrow), platelet trabeculae (black arrow) and inflammatory cells (gray arrow), were observed in the lumen. Numerous infiltrating inflammatory cells (gray arrow) were observed in the media or adventitia.

Moreover, the number of iron spots (stained blue) increased, and the spots were widely distributed in the vascular tissues (Fig. 1G). The quantitative assessment of iron levels showed that there was obvious overload of iron in vascular tissues after mechanical injury-related DVT formation, which was approximately 5.7 times greater than that in the sham group (Fig. 1H, $P < 0.0001$; unpaired *t*-test). DHE fluorescence staining and ROS fluorescence intensity indicated significant ROS accumulation in the veins of the DVT group compared with those of the sham group (Fig. 1I, red fluorescence signal; Fig. 1J, $P < 0.01$). Hypoxia inducible factor-1 (HIF1α) was upregulated in the samples from the DVT group (Fig. S1C).

3.2. Confirmation that ferroptosis is key pathway and TFRC is a hub protein associated with thrombus formation via WGCNA

A protein co-expression network was successfully constructed by WGCNA (Fig. 2, Fig. S1E). A total of 2007 proteins identified in the label-free quantitative proteomics were divided into 16 color modules (Fig. 2A). Significance and correlation analyses of all the color modules and thrombus formation were performed (Fig. 2B and C). The blue module had the most significant positive correlation with thrombosis formation (Fig. 2B, $R = 0.999$), while the turquoise module had a significant negative correlation with thrombosis (Fig. 2B, $R = -0.993$). As shown in Fig. 2D, we found that TFRC was a hub protein that is involved in thrombus formation. Moreover, abnormal expression of proteins that regulate iron homeostasis was observed in the DVT group (Fig. 2E). The protein expression of TFRC in injured FVs was markedly upregulated in the DVT group compared to the control group (Mann–Whitney *U* test, $P = 0.0286$), as shown in Fig. 2F. TFRC, as well as its role in the regulation of iron homeostasis, may be crucial for thrombogenesis after venous mechanical injury. In addition, THBS1 was one of the most significantly expressed proteins according to our differential analysis. Predictions of

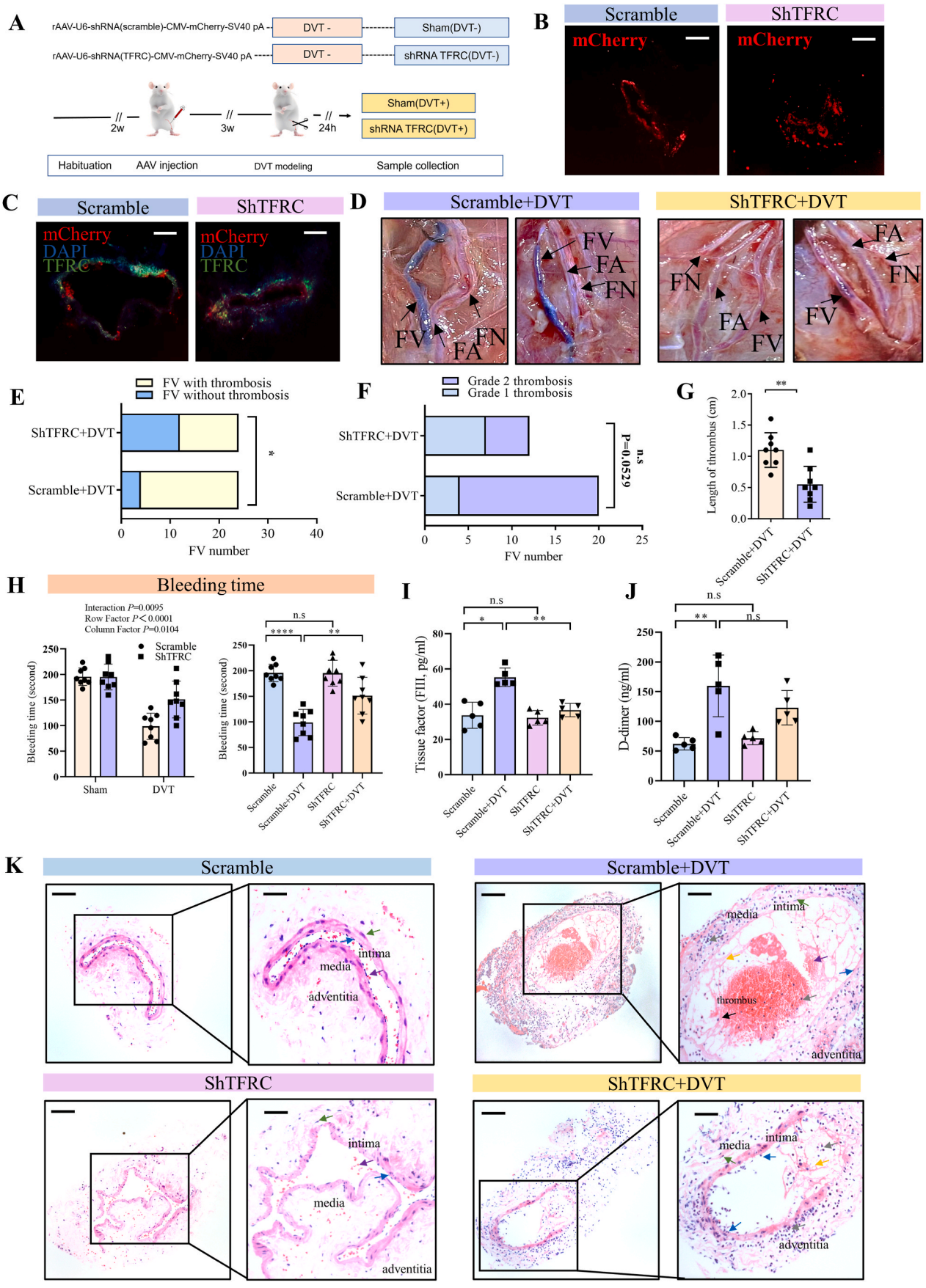

(caption on next page)

Fig. 3. Iron accumulation mediated by TFRC contributes to thrombosis in injured femoral veins (FVs). (A) Schematic representation of reverse conditional intervention targeting TFRC in DVT models. (B) Fluorescence images of mCherry in the scramble and shTFRC groups. (C) Fluorescence staining for TFRC in the scramble and shTFRC groups. Representative images from n = 3 rats/group are shown, and the scale bar in the fluorescence images is 100 μm. (D) Gross observation of DVT, where FV = femoral vein, FA = femoral artery, and FN = femoral nerve. (E) Thrombosis rate, n = 24. (F), Proportion of Grade 1 and Grade 2 thrombi in the scramble + DVT (n = 20) and shTFRC + DVT (n = 12) groups. (G) Length of thrombus (n = 8). In Fig. E and F, the values are expressed as the percentage of classified veins (with/without thrombosis; grade 1/2 thrombosis). "*" ($P < 0.05$) and "n.s" ($P > 0.05$, nonsignificant) indicate a marked difference based on Fisher's exact test. In Fig. G, the values are expressed as the mean ± SD of replicates. "**" ($P < 0.01$) indicates a significant difference according to the T test. (H) Bleeding time (n = 8); statistical analysis was performed with one-way ANOVA and t tests; "**" ($P < 0.01$), "***" ($P < 0.001$), or "****" ($P < 0.0001$) indicates a significant difference according to the *t*-test. (I) ELISA analysis of the level of plasma tissue factor in rats from the various groups; n = 5. The values are expressed as the mean ± SD of replicates, and statistical analysis between two groups with the same variants was performed with the Mann–Whitney *U* test. (J) ELISA analysis of the plasma D-dimer level in rats in the various groups; n = 5. The values are expressed as the mean ± SD of replicates, and statistical analysis was performed with the Kruskal-Wally test. (K) Pathological changes in tissues (n = 3). All the samples were cross-sectioned. The scale bar indicates 100 and 50 μm at low and high magnification, respectively. Endothelial cells (shown by the blue arrow), red blood cells (purple arrow), platelet trabeculae (black arrow), fibrin (orange arrow), vascular smooth muscle cells (green arrow) and inflammatory cells (gray arrow) were observed. (For interpretation of the references to color in this figure legend, the reader is referred to the Web version of this article.)

the PROPER dataset, which is a human PPI reference network generated by PROER-seq, showed that TFRC may interact with THBS1 in HUVECs (Fig. 2G).

The pathology of DVT is very complicated and involves multiple metabolic and cellular processes, including carbon metabolism, lipid metabolism, and genetic translation (Fig. S2A). In particular, the pathological changes caused by upregulated proteins were associated with multifarious pathways, such as "complement/coagulation cascades", "regulation of the actin cytoskeleton", "neutrophil extracellular trap formation", "focal adhesion", "leukocyte transendothelial migration" and "ferroptosis". Figure A shows that "cell growth and death" was enriched. In this study, ferroptosis was the 14th pathway of the top 30 pathways that were identified by KEGG enrichment analysis (Fig. S2B). The results indicated that ferroptosis was the most highly enriched cell death pathway, and the ratio of genes related to ferroptosis was higher than that of genes related to necroptosis, apoptosis, autophagy and mitophagy (Fig. S2C). As for other pathways, hypoxia in injured femoral veins may be reflected by the HIF1 signaling pathway activation (Table S1).

3.3. TFRC contributes to thrombosis in injured FVs

Based on reverse conditional intervention, we conditionally knocked down TFRC expression (Fig. 3A). To avoid excessive systemic intervention, we compared two AAV injection methods: AAV injection with or without blood supply blockade. Blocking the blood supply of FVs after AAV injection prevented effects on iron intake in the liver, heart and inferior vena cava to a certain extent (Figs. S3A and B). After three weeks of treatment, distinct mCherry fluorescence, which is the reporter protein expressed by the AAV vector, was observed in the frozen sections of FVs from the scramble and shTFRC groups (Fig. 3B). These findings indicated that the AAV system successfully accumulated in FVs. Immunofluorescence analysis revealed that the expression of TFRC was efficiently knocked down in FV tissues (Fig. 3C).

A DVT model was established by mechanical injury (Fig. 3D). In the AAV interference experiment, 12 rats were included in each group, and the bilateral femoral vein on both sides was included in model establishment; thus, the number of affected femoral veins was 24. All the venous tissues were included in further experiments. Knocking down TFRC affected thrombogenesis, and the formation rates of the scramble + DVT and shTFRC + DVT groups were 83.3 % (20/24) and 50 % (12/24), respectively, which were significantly different (Fig. 3E; Fisher's exact test, $P = 0.0305$). As shown in Fig. 3F, Grade 2 thrombi were frequently observed in the scramble + DVT group (16/20, 80 %) but were infrequently observed in the shTFRC + DVT group (5/12, 41.6 %), and the difference between the two groups was almost significant (Fisher's exact test, $P = 0.0529$). Compared with that in the scramble + DVT group, the total length of the thrombus in the shTFRC + DVT group was decreased (Fig. 3G, $P = 0.0016$). In all the DVT groups, compared with those in the scramble + DVT group, the loss of TFRC increased caudal vein bleeding time and reduced the level of tissue factor (FIII) (Fig. 3H, two-way ANOVA test, interaction: $P = 0.0095$, row factor: $P < 0.0001$, column factor $P = 0.0104$; $P < 0.01$, T test; Fig. 3I; $P < 0.05$); however, the D-dimer level was not significantly different (Fig. 3J). Changes in the tissue were observed by histopathological analysis (Fig. 3K). The pathological description of each group is given below.

Scramble group: No obvious thrombi were evident in the vascular lumen, the structures of the vascular intima and endothelial cells were normal, and no obvious shedding was observed. No obvious inflammatory cell infiltration was observed in the vascular media or adventitia.

Scramble + DVT group: The vascular endothelium was damaged, and few obvious endothelial cells were observed (blue arrow). Mixed large thrombi, which consisted of red blood cells (purple arrow), platelet trabeculae (black arrow), fibrin (orange arrow) and inflammatory cells (gray arrow), were observed in the lumen. Numerous inflammatory cell infiltrates were observed in the media or adventitia.

ShTFRC group: No pathological changes were observed. Pathological impressions of the shTFRC group were similar to those of the scramble group.

ShTFRC + DVT group: The number of endothelial cells (blue arrow) was reduced, but a small number of these cells were still present. No obvious thrombus was evident in the lumen, except for the fibrin network (orange arrow). High levels of inflammatory cell infiltration (gray arrow) were observed in the media and adventitia.

3.4. TFRC knockdown inhibits iron overload, redox bursts and ferroptosis in injured FVs

The ROS signal in the scramble + DVT group was more intense than that in the scramble, shTFRC and shTFRC + DVT groups, indicating an increase in ROS bursts in the injured veins (Fig. 4A). TFRC knockdown inhibited redox bursts in injured FVs, and the level of ROS in tissues was significantly increased in the scramble + DVT group but was reduced after TFRC was knocked down (Fig. 4B, $P < 0.05$). Accordingly, compared with that in the scramble and shTFRC groups, the intensity of GSH fluorescence was lower in the scramble + DVT group (Fig. 4C). The fluorescence results were consistent with the changes in the quantitative data. In the tissue samples, there was a significant difference between the AAV interference group and the DVT model group (Fig. 4D, one-way ANOVA). Silencing TFRC markedly reversed GSH depletion in tissue and serum samples ((Fig. 4D and E), reduced the level of GSSG and increased the GSH/GSSG ratio after thrombosis (Fig. 4F, G, $P < 0.05$) in tissue samples. MDA contents were strongly increased in the scramble + DVT group and reduced in the shTFRC group (Fig. 4H, Mann–Whitney *U* test). The MMP of the FV tissues was markedly reduced after mechanical injury, and silencing of TFRC reversed this effect (Fig. 4I).

As shown in Fig. 5A, ferric ions (Fe^{3+}) were identified as blue granules and were widely distributed in the intima, media and adventitia of injured veins in the absence of AAV. Loss of TFRC significantly limited iron intake in venous tissues (black arrows). Iron levels were

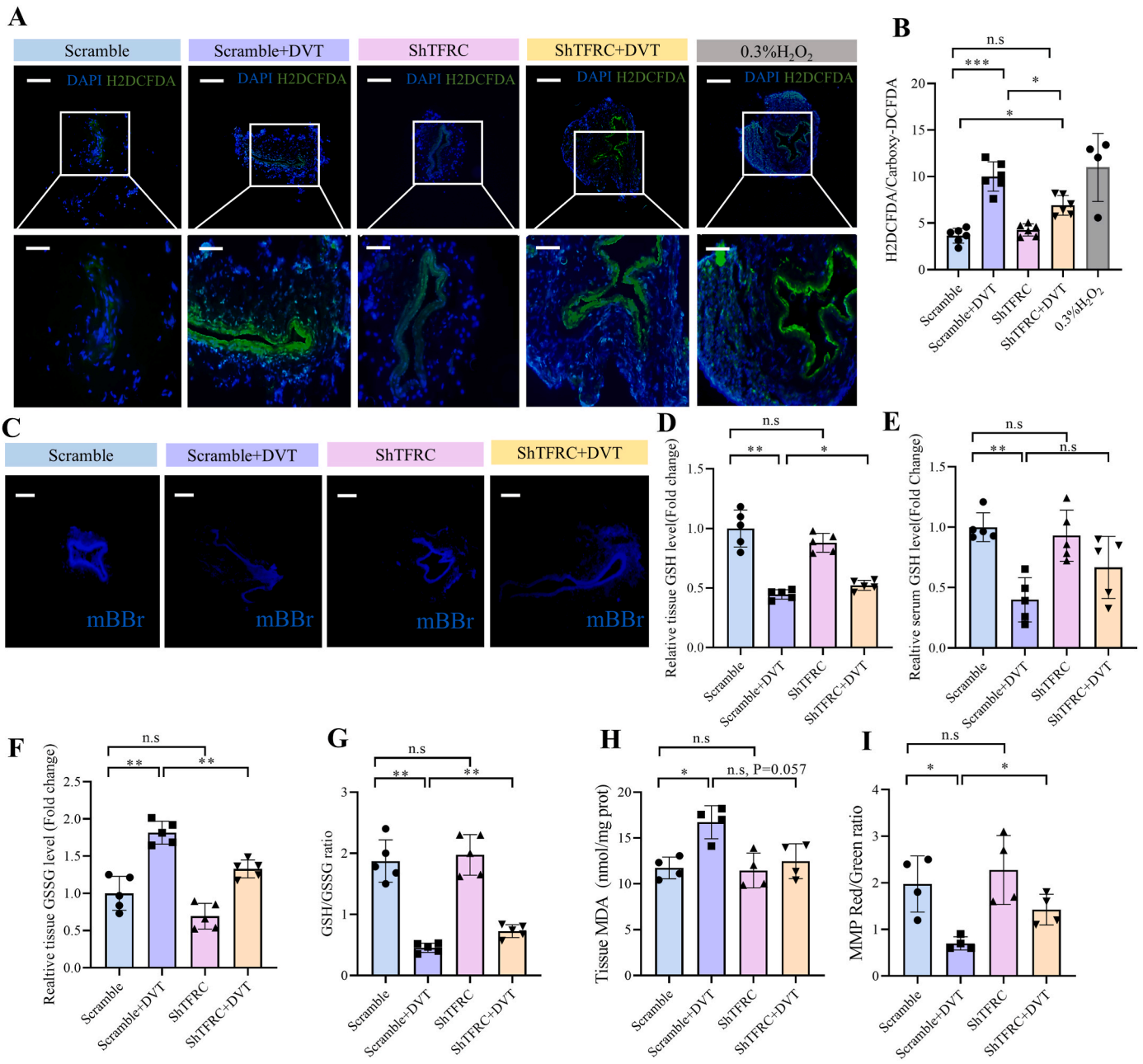

Fig. 4. TFRC knockdown inhibits redox bursts in mechanically injured FVs. (A) Fluorescence staining for ROS; n = 3. All the samples were cross-sectioned. The scale bar indicates 100 and 50 μm at low and high magnification, respectively. Treatment with 0.3 % H_2O_2 was used as a positive control. (B) Measurement Tissue ROS levels were quantified by H_2DCFDA/carboxy-DCFDA, n = 4~6, and the values are expressed as the mean ± SD of replicates. Statistical analysis of the differences between groups with a single variable was performed with one-way ANOVA; "*" ($P < 0.05$) or "*0*" ($P < 0.001$) indicates a significant difference while "n.s" indicates a nonsignificant difference according to the Mann−Whitney *U* test. (C) Fluorescence staining for GSH; n = 3. All the samples were cross-sectioned. The scale bar indicates 100 μm. (D) Relative tissue GSH levels; n = 5. The values are expressed as the mean ± SD of replicates, and the statistical analysis between two groups with the same variants was performed with the Mann−Whitney *U* test; "*" ($P < 0.05$) or "**" ($P < 0.01$) indicates a significant difference while "n.s" indicates a nonsignificant difference. (E) Relative serum GSH levels; n = 5. The values are expressed as the mean ± SD of replicates, and the statistical analysis between two groups with the same variants was performed with the Mann−Whitney *U* test; "**" ($P < 0.01$) indicates a significant difference. And "n.s" indicates a nonsignificant difference. (F) Relative tissue GSSG levels; n = 5. The values are expressed as the mean ± SD of replicates, and the statistical analysis between two groups with the same variants was performed with the Mann−Whitney *U* test; "**" ($P < 0.01$) indicates a significant difference, and "n.s" indicates a nonsignificant difference. (G) Relative ratio of GSH/GSSG, n = 5. The values are expressed as the mean ± SD of replicates, and the statistical analysis between two groups with the same variants was performed with the Mann−Whitney *U* test; "**" ($P < 0.01$) indicates a significant difference, and "n.s" indicates a nonsignificant difference. (H) Quantitative measurement of tissue MDA levels; n = 4~5. The values are expressed as the mean ± SD of replicates, and the statistical analysis of two groups with the same variants was performed with the Mann−Whitney *U* test; "*" ($P < 0.05$) indicates a significant difference, and "n.s" indicates a nonsignificant difference. (I) Quantitative measurement of the MMP rate; n = 4. The values are expressed as the mean ± SD of replicates, and the statistical analysis between two groups with the same variants was performed with the Mann−Whitney *U* test; "*" ($P < 0.05$) or "**" ($P < 0.01$) indicates a significant difference, and "n.s" indicates a nonsignificant difference.

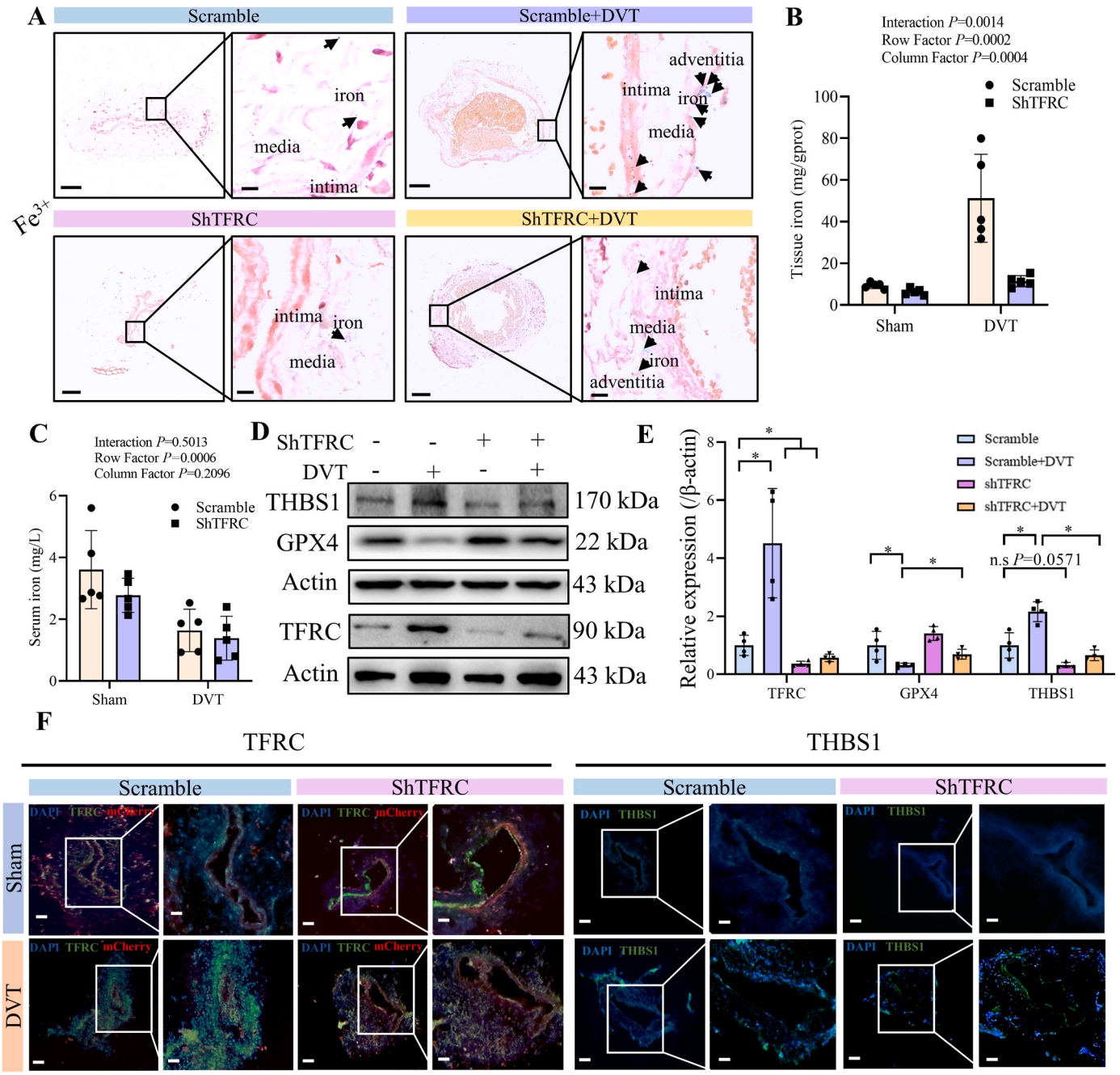

Fig. 5. TFRC knockdown reduces iron overload and inhibits ferroptosis in mechanically injured FVs. (A) Perl staining (n = 3) showing the iron (Fe^{3+}) contents in vascular tissues (black arrows); the scale bar indicates 100 and 10 μm at low and high magnification, respectively. All the samples were cross-sectioned. (B) Results from the quantitative measurement of total iron concentrations in the tissue (Fe^{3+}, Fe^{2+}), n = 5; the values are expressed as the mean ± SD of replicates, and statistical analysis was performed with two-way ANOVA. (C) Quantitative measurement of the total serum iron concentration (Fe^{3+}, Fe^{2+}), n = 5. The values are expressed as the mean ± SD of replicates, and statistical analysis was performed with two-way ANOVA. (D) The protein expression of THBS1 (~170 kDa), TFRC (~90 kDa) and GPX4 (~22 kDa) in venous tissues from the scramble and shTFRC groups and the protein expression of THBS1 (~170 kDa), TFRC (~90 kDa) and GPX4 (~22 kDa) after TFRC knockdown in venous tissues from the DVT groups were determined; β-actin (~43 kDa) was used as a loading control (n = 4). (E) Quantification of the data in Fig. 5D. Protein levels were normalized to actin levels (n = 4). The values are expressed as the mean ± SD of replicates. "*" ($P < 0.05$) or "**" ($P < 0.01$) indicates a significant difference and "n.s" ($P > 0.05$) indicates a nonsignificant difference between two groups according to the Mann–Whitney *U* test. (F) Immunofluorescence staining for TFRC and THBS1 in the various groups (n = 3). The scale bar indicates 100 and 50 μm at low and high magnification, respectively. All the samples were cross-sectioned.

markedly increased in the tissues of the scramble + DVT group and reduced in those of the AAV interference groups (Fig. 5B). A similar trend was observed in the serum samples (Fig. 5C).

Western blotting analysis revealed that TFRC was successfully silenced after AAV interference (Fig. 5D and E). This interference also reversed the increase in TFRC expression after DVT induction. The expression of GPX4 was markedly downregulated in the scramble + DVT group compared to the control group ($P < 0.05$). Moreover, GPX4 expression was significantly increased in the shTFRC + DVT group. These findings indicated that TFRC knockdown efficiently inhibited ferroptosis. THBS1, the thrombogenesis-related protein of interest, was highly expressed in the DVT model. Interestingly, TFRC knockdown also

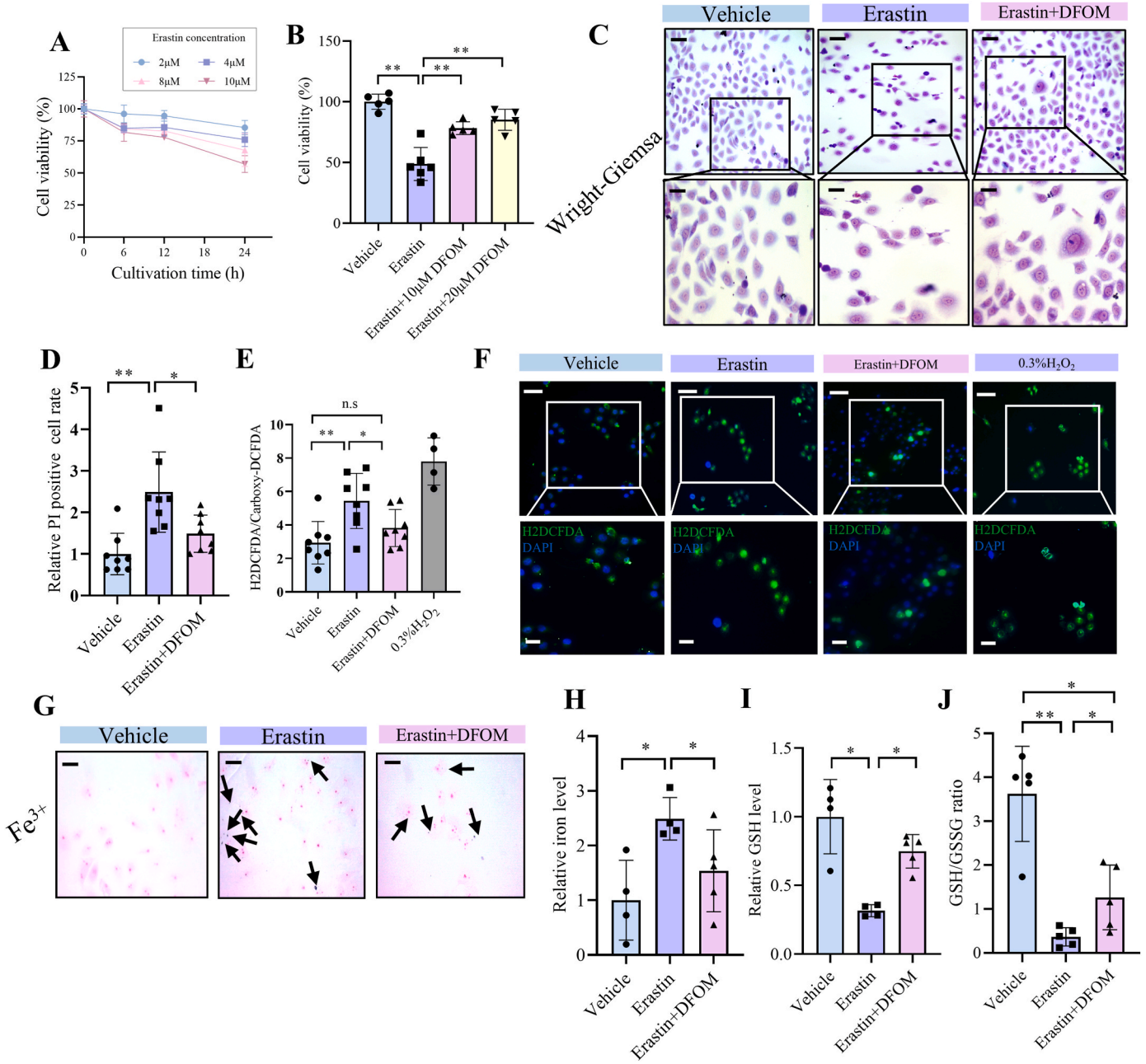

Fig. 6. Erastin-induced ferroptosis interferes with redox and iron homeostasis in HUVECs. (A) Inhibition curve of HUVECs treated with different concentrations of erastin (n = 5). (B) CCK8 analysis of HUVECs after various treatments; n = 5~6, and statistical analysis between two groups with the same variants was performed with the Mann–Whitney *U* test, "*" ($P < 0.05$), "**" ($P < 0.01$) indicate a significant difference. (C) Observation of morphology by Wright–Giemsa staining; n = 3. The scale bar indicates 200 and 100 μm at low and high magnification, respectively. (D) Relative proportion of PI-positive cells, n = 8. The values are expressed as the mean ± SD of replicates. Statistical analysis between two groups with the same variants was performed with the Mann–Whitney *U* test, "**" ($P < 0.01$), "***" ($P < 0.001$) indicates a significant difference according to the Mann–Whitney *U* test. (E) ROS fluorescence was quantified by H_2DCFDA/carboxy-DCFDA, n = 8 (n = 4 in the positive control). The values are expressed as the mean ± SD of replicates, and statistical analysis between two groups with the same variants was performed with the Mann–Whitney *U* test, "**" ($P < 0.01$) or "***" ($P < 0.001$) indicates a significant difference (F) ROS fluorescence staining, n = 3. DAPI was used to stain the cell nucleus. The scale bar indicates 200 and 100 μm at low and high magnification, respectively. Treatment with 0.3 % H_2O_2 was used as a positive control. (G) Perl staining (n = 3) showing the iron (Fe^{3+}) contents in HUVECs (black arrows), and eosin staining of the cytoplasm; the scale bar indicates 200 μm. (H) Relative iron (Fe^{3+} and Fe^{2+}) levels; n = 4~5. The values are expressed as the mean ± SD of replicates, and statistical analysis between two groups with the same variants was performed with the Mann–Whitney *U* test, "*" ($P < 0.05$) or "**" ($P < 0.01$) indicates a significant difference. (I) GSH levels in HUVECs under different interference conditions; n = 4~5. The values are expressed as the mean ± SD of replicates; and statistical analysis between two groups with the same variants was performed with the Mann–Whitney *U* test, "*" ($P < 0.05$) or "**" ($P < 0.01$) indicates a significant difference. (J) Relative ratio of GSH/GSSG, n = 5. The values are expressed as the mean ± SD of replicates, and the statistical analysis between two groups with the same variants was performed with the Mann–Whitney *U* test; "*" ($P < 0.05$) and "**" ($P < 0.01$) indicates a significant difference.

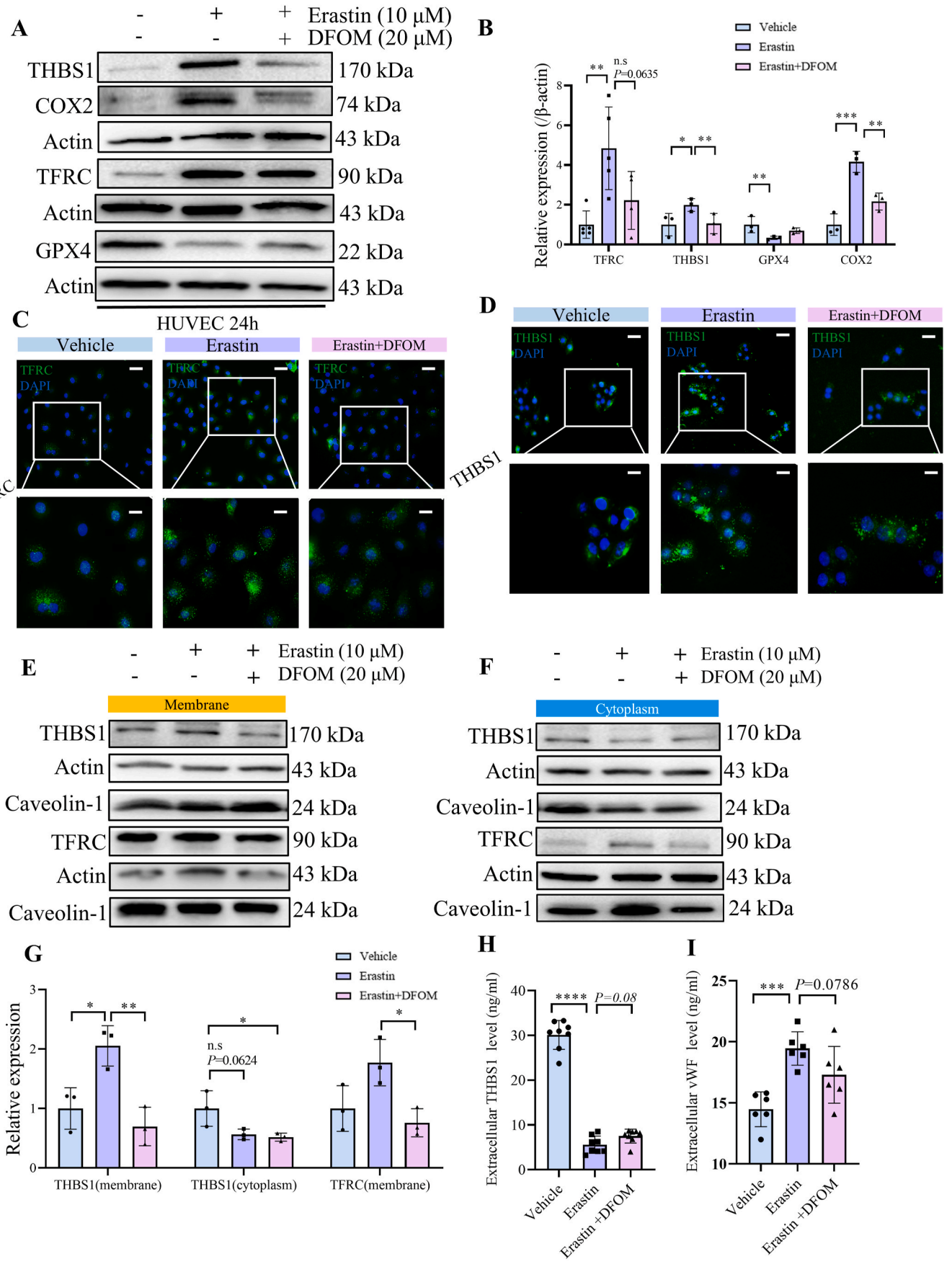

(caption on next page)

Fig. 7. Erastin-induced ferroptosis interferes with TFRC expression and THBS1 secretion by HUVECs.
(A) Western blotting (n = 3) was used to determine the expression of THBS1 (~170 kDa), TFRC (~90 kDa), COX2 (~74 kDa) and GPX4 (~22 kDa), and β-actin (~43 kDa) was used as a loading control. (B) Quantification of protein levels; the data were normalized to actin levels (n = 3~5). The values are expressed as the mean ± SD of replicates; "*" ($P < 0.05$), "**" ($P < 0.01$), or "***" ($P < 0.001$) indicates a significant difference, and "n.s" ($P > 0.05$) indicates a nonsignificant difference between two groups with one single variate according to one-way ANOVA. (C) Immunofluorescence staining for TFRC in the various groups (n = 3). The scale bar indicates 100 μm and 50 μm at low and high magnification, respectively. All the samples were cross-sectioned. DAPI was used to stain the cell nucleus. (D) Immunofluorescence staining for THBS1 in the various groups (n = 3). The scale bar indicates 100 μm and 50 μm at low and high magnification, respectively. All the samples were cross-sectioned. DAPI was used to stain the cell nucleus. (E) Western blotting (n = 3) was used to determine the expression of THBS1 (~170 kDa) and TFRC (~90 kDa) in the cell membrane. Caveolin-1 (~24 kDa) was used as a loading control. (F) Western blotting (n = 3) was used to determine the expression of THBS1 (~170 kDa) and TFRC (~90 kDa) in the cytoplasm. β-Actin (~43 kDa) was used as a loading control. (G) Quantification of the data was performed by normalization to actin or caveolin-1 expression (n = 3); the values are expressed as the mean ± SD of replicates; "*" ($P < 0.05$) or "**" ($P < 0.01$) indicates a significant difference and "n.s" ($P > 0.05$) indicates a nonsignificant difference between two groups with one single variate according to one-way ANOVA. (H) ELISA analysis of extracellular THBS1 levels; n = 8. The values are expressed as the mean ± SD of replicates, and statistical analysis between two groups with the same variants was performed with the Mann–Whitney *U* test, "*" ($P < 0.05$) and "****" ($P < 0.0001$) indicate a significant difference. (I) ELISA analysis of extracellular vWF levels; n = 6. The values are expressed as the mean ± SD of replicates. "***" ($P < 0.001$) indicates a significant difference between two groups according to the *t*-test.

downregulated THBS1 in the shTFRC and shTFRC + DVT group. This finding suggested that TFRC may regulate or interact with THBS1. Immunofluorescence images revealed the location of TFRC and THBS1. TFRC was mainly expressed in the endangium and tunica adventitia, while THBS1 was primarily expressed in the endangium (Fig. 5F, Fig. S3C).

3.5. TFRC and THBS1 are sensitive to erastin-induced ferroptosis in HUVECs

As shown in Fig. 6A, compared with vehicle treatment, erastin treatment resulted in substantial cell death, as indicated by a 50 % inhibition concentration of 10 μM after 24 h (Fig. 6B). A concentration of 20 μM DFOM had little effect on the normal growth of HUVECs (Fig. S4A). Conversely, cells incubated with DFOM exhibited increased resistance to erastin (Fig. 6B). Wright–Giemsa staining revealed that the cell density in the erastin group was lower than that in the vehicle and DFOM groups. However, there were no distinct differences in morphology (Fig. 6C). PI staining showed that the number of dead HUVECs was increased by erastin treatment, and DFOM inhibited cell death to a certain extent ($P < 0.01$; Fig. 6D). Erastin treatment exacerbated the ROS burst, and DFOM significantly inhibited ROS accumulation (Fig. 6E and F, $P < 0.01$). Many blue granules of iron (Fe^{3+}) were observed in cells in the erastin group, and DFOM efficiently chelated these iron ions (Fig. 6G, black arrows). Compared with those in the vehicle control group, the relative iron levels in the erastin group were markedly increased by 250 %; in addition, these levels were decreased by approximately 37.9 % after DFOM treatment (Fig. 6H, $P < 0.05$). Accordingly, the GSH levels were lower in erastin-treated cells than in control cells (Fig. 6I; Mann–Whitney *U* test, $P < 0.05$). DFOM markedly increased the GSH levels and the GSH/GSSG ratio after erastin treatment (Fig. 6I, J, $P < 0.05$). Then, the protein expression of ferroptosis markers was measured. As shown in Fig. 7A and B, the expression of GPX4 was downregulated in the erastin group compared to the vehicle group ($P < 0.01$). Compared with that in the erastin group, the expression of GPX4 in the DFOM treatment group was upregulated to a certain extent, but this difference was not significant (Fig. 7B). COX2 expression was upregulated in erastin-treated cells but was markedly downregulated by DFOM treatment (Fig. 7B, $P < 0.01$). Interestingly, THBS1 and TFRC were highly expressed in the erastin-treated group (Fig. 7A and B). These changes in THBS1 expression in the in vitro ferroptosis model are consistent with the changes that were observed in DVT tissues. The expression of THBS1 was affected by erastin treatment in a dose-dependent manner, similar to the changes in the expression of TFRC, and this treatment had the opposite effect on GPX4 (Fig. S4B). Immunofluorescence (Fig. 7C and D) and Western blotting results showed that TFRC and THBS1 were expressed on the membrane and in the cytoplasm, respectively, and that their expression was upregulated in response to erastin (Fig. 7E, F, 7G). The level of THBS1 on the membrane was significantly increased after erastin treatment (Fig. 7G, $P < 0.05$), and DFOM treatment reversed this effect. The secretion of THBS1 was significantly affected by ferroptosis. Compared with that in the vehicle group, the level of extracellular THBS1 was reduced ($P < 0.0001$) and recovered after ferroptosis was inhibited (Fig. 7H). Secreted THBS1 plays a crucial role in hemostasis, especially through its ability to cleave vWF. ELISA analysis indicated that extracellular vWF was overproduced by HUVECs under ferroptotic conditions (Fig. 7I, $P < 0.001$).

3.6. TFRC knockdown reverses ferroptosis and THBS1 protein level in HUVECs

To elucidate the underlying role of TFRC in the progression of ferroptosis and the regulation of THBS1 levels, TFRC was knocked down in HUVECs. Based on the growth curve of HUVECs exposed to puromycin dihydrochloride, the optimal screening concentration of puromycin dihydrochloride was determined to be approximately 2 μg/ml (Figs. S4D and 4E). Then, clones stably expressing shTFRC were successfully generated (Fig. S4F). We examined the levels of a series of ferroptosis indicators and target proteins. After TFRC was knocked down, the expression of proteins that promote ferroptosis (COX2 and TFRC) was significantly downregulated (Fig. 8A and C). We were surprised by the effects of TFRC knockdown on THBS1 expression because the latter was also downregulated in the control group (Fig. 8B and C). TFRC knockdown also reversed erastin-induced ferroptosis, and cell viability increased from 57.8 to 77.5 % (Fig. 8D and E). However, complete knockdown TFRC alone reduced cell viability to 38 % (Fig. 8F). Therefore, the loss of TFRC tends to be lethal in HUVECs, and we decreased the knockout efficiency by regulating the MOI that was used for viral transduction. Then, TFRC knockdown reversed ferroptosis. The accumulation of ROS and iron was significantly reduced in TFRC-knockdown cells treated with erastin (Fig. 8G and H). Unexpectedly, the level of extracellular THBS1 did not align with the change in intracellular THBS1 expression. After silencing TFRC, the intracellular THBS1 level was reduced, but THBS1 secretion was increased (Fig. 8I; two-way ANOVA test; interaction: $P = 0.0008$, row factor: $P < 0.0001$, column factor: $P < 0.0001$). Changes in the expression of several ferroptosis proteins were also detected (Fig. 8J-L). With the knockdown of TFRC, the level of THBS1 also decreased in the erastin-treated group (Fig. 8K, L).

3.7. TFRC interacts with THBS1

TSA-based double immunofluorescence staining revealed the colocalization of TFRC and THBS1 in HUVECs (Fig. 9A). The fluorescence curve of TFRC (red) almost coincided with that of THBS1 (Fig. 9B). Through Z-docking, we selected ten potential poses (Table S2). The accurate Rdock docking results showed that the E_rdock energy score of Pose 9 was −27.5056, which was the lowest among all the tested poses,

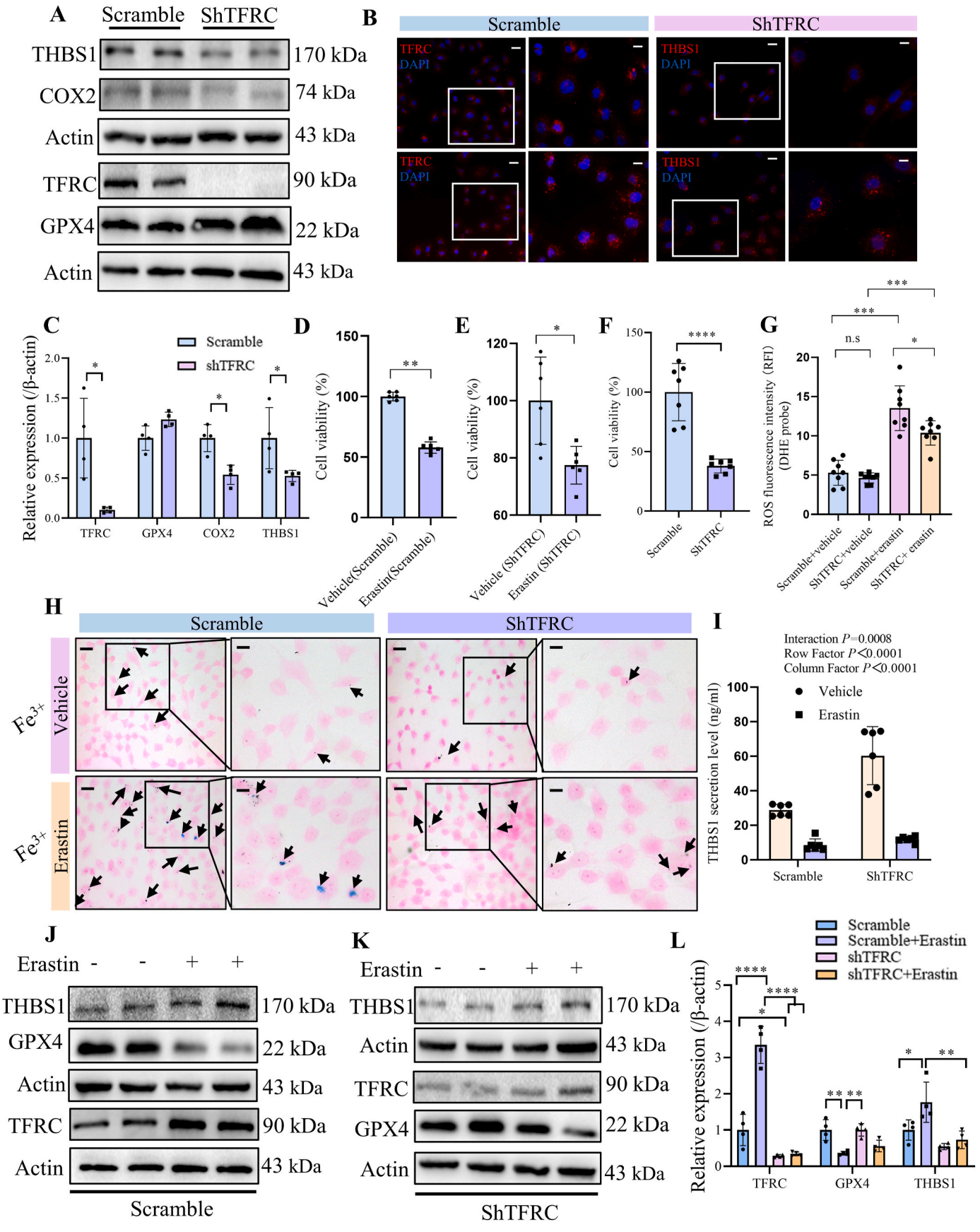

(caption on next page)

Fig. 8. TFRC knockdown reverses the level of THBS1 and reduces the sensitivity of HUVECs to erastin-induced ferroptosis. (A) Western blotting (n = 4) was used to determine the expression of THBS1 (~170 kDa), TFRC (~90 kDa), COX2 (~74 kDa) and GPX4 (~22 kDa) in scramble- or shTFRC-transfected HUVECs. β-Actin (~43 kDa) was used as a loading control. (B) Immunofluorescence staining for TFRC and THBS1 in scramble and shTRFC cells (n = 3). DAPI was used to stain the cell nucleus. The scale bar indicates 100 and 50 μm at low and high magnification, respectively. (C) Quantification of the data in Fig. 7A. The protein levels were normalized to the actin level (n = 4); the values are expressed as the mean ± SD of replicates, and "*" ($P < 0.05$) indicates a significant difference between two groups according to the Mann–Whitney *U* test. (D) Cell viability of the scramble and shTFRC (TFRC was completely knocked out) groups (n = 7). (E) Viability of HUVECs in the scramble groups after treatment with DMSO or erastin (n = 6). (F) Viability of HUVECs in the shTFRC groups after treatment with DMSO or erastin (n = 6). For (D), (E) and (F), the values are expressed as the mean ± SD of replicates, and "*" ($P < 0.05$), "**" ($P < 0.01$), and "****" ($P < 0.0001$) indicate a significant difference according to the *t*-test. (G) ROS fluorescence (DHE probe) quantification; n = 8. The values are expressed as the mean ± SD of replicates. "**" ($P < 0.01$) or "***" ($P < 0.001$) indicates a pairwise comparison difference according to the Mann–Whitney *U* test. (H) Perl staining (n = 3) showing the iron (Fe^{3+}) contents in the scramble and shTFRC groups treated with or without erastin (black arrows); eosin stains the cytoplasm, and the scale bar indicates 100 and 50 μm at low and high magnification, respectively. (I) ELISA analysis of the extracellular THBS1 levels in the scramble and shTFRC groups after treatment with or without erastin; n = 6. The values are expressed as the mean ± SD of replicates, and statistical analysis was performed with two-way ANOVA. (J) The protein expression of THBS1 (~170 kDa), TFRC (~90 kDa) and GPX4 (~22 kDa) in HUVECs in the scramble groups was assessed with or without erastin interference, and β-actin (~43 kDa) was used as a loading control (n = 4). (K) The protein expression of THBS1 (~170 kDa), TFRC (~90 kDa) and GPX4 (~22 kDa) in HUVECs in the shTFRC groups, with or without erastin interference, and β-actin (~43 kDa) was used as a loading control (n = 4). (L) Quantification of the data in Fig. 7J and K. Protein levels were normalized to actin levels (n = 4); the values are expressed as the mean ± SD of replicates. "*" ($P < 0.05$), "**" ($P < 0.01$) or "****" ($P < 0.0001$) indicates a significant difference between two groups according to the Mann–Whitney *U* test.

indicating that this pose was the most stable (Table S2). As shown in Fig. 8C and Figs. S5A and 4B, the green molecule is TFRC, and the sky-blue molecule is THBS1. The red dashed line in Fig. S5C represents the hydrogen bond. TFRC and THBS1 were successfully docked, and the free energy was −9.8, indicating that the docking result was meaningful. For instance, GLN320, SER472, TYR683, TYR689, ARG698, and ASN758 of TFRC form hydrogen bonds with ASP502, GLY533, CYS533, ASP530, GLY528, GLY527, and LYS486 of THBS1 (Fig. 9C). Thus, our molecular docking results indicated that TFRC could interact with THBS1 through multiple hydrogen bonds (Fig. 9C, Fig. S5C), and the detailed results are shown in Table S3. Co-IP analysis further verified this interaction. As shown in Fig. 9D and E, a potential interaction occurred between TFRC and THBS1 in HUVECs. The binding domain was located mainly among the regions of TSR1-2 and TSR1-3 in THBS1 (Fig. 9F and G).

3.8. Ferroptosis affects the interaction between TFRC-THBS1and THBS1-CD47

Moreover, the interaction between TFRC and THBS1 was affected by erastin treatment (Fig. 9D–E). Specifically, erastin treatment impaired the interaction between TFRC and THBS1. In addition, as the binding agent decreased with increasing erastin treatment duration, the colocalization curves were separated, the fluorescence pixels in the two channels were dispersed, and the R coefficient of the interaction was reduced from an average of 0.835 to an average of 0.58 after 24 h of culture (Fig. 10A–D). As shown in Fig. 10E, two colocalization coefficients were greater in the sham group (R = 0.93, overlap = 0.93) but were lower in the DVT group (R = 0.68, overlap = 0.68). We subsequently analyzed the effect of the ferroptosis inhibitor on the interaction in venous tissues (Fig. 10F), which was verified via co-IP analysis. We found that after DVT model establishment, the intensity of the IP bands corresponding to TFRC-immunoprecipitated THBS1 was reduced. These results are consistent with the colocalization of TFRC and THBS1 in venous tissues and thrombus formation in vivo and in vitro. Moreover, the inhibition of ferroptosis by liproxstatin-1 reversed these effects in vivo (Fig. 10G and H).

The transferrin transfer ability of TFRC can be enhanced during ferroptosis. We hypothesized that a natural ligand of TFRC, transferrin, may compete with THBS1 for interaction with TFRC. Thus, transferrin was added to the culture environment. A low dose of TRF promoted the proliferation of HUVECs but did not induce ferroptosis (Fig. S5D, $P < 0.05$; Fig. S5E). The binding of transferrin to TFRC weakened the binding of TFRC to THBS1 during ferroptosis (Fig. S5F).

What consequences will a weakened interaction between TFRC and THBS1 have? We found that the binding domain was located mainly within the regions of TSR1-2 and TSR1-3 in THBS1 (Fig. 9F and G). The binding site of CD36 is also close to this domain. CD36 is a natural receptor of THBS1, and it shares a similar THBS1 binding domain with TFRC. However, an early report showed that CD36 was not expressed by HUVECs [20]. Therefore, we investigated the role of another important natural ligand of THBS1, CD47, in the interaction of THBS1 during ferroptosis with or without TFRC knockdown. First, the localization of CD47 and THBS1 was highly enhanced in venous tissues during thrombogenesis (Fig. 11A and B). However, neither erastin treatment nor TFRC knockdown affected the expression of CD47 in HUVECs (Fig. 11C and D). The colocalization results indicated that the colocalization intensity of THBS1 and CD47 was increased to a certain extent in HUVECs undergoing ferroptosis (Fig. 11E–G, H), while TFRC knockdown reversed this effect (Fig. 11F, G, H).

4. Discussion

In this study, we further hypothesized that TFRC not only affected thrombus formation by regulating iron accumulation but also influenced the THBS1 protein. To verify these hypotheses and explore the therapeutic effect of TFRC on DVT, injury was induced in rat femoral veins to establish a DVT model. Iron overload was present in venous tissues with thrombosis. We demonstrated that TFRC serves as a hub protein and is highly expressed in veins with DVT. The knockdown of TFRC alleviated iron overload and oxidative stress, consequently reducing ferroptosis and thrombus formation in the injured venous tissue. THBS1 was upregulated in DVT tissues, and the loss of TFRC decreased its protein level. We further verified these findings in human cells. Similar changes in the expression of TFRC and THBS1 were observed in classic ferroptosis models, and these factors were highly expressed in the whole cell and cellular membrane in the presence of erastin. The effect of DFOM and TFRC knockdown reversed these results. The in vitro experiments indicated that the release of THBS1 was reduced after erastin administration, and there was a robust increase in extracellular vWF levels. Knocking down TFRC could increase extracellular THBS1, which assured us that these two proteins could interact with each other. The prediction based on the PROPER PPI network and molecular docking and a series of biochemical experiments verified our hypothesis; that is, TFRC can interact with THBS1. In addition, treatment with erastin (in vitro) or DVT construction (in vivo) decreased the binding efficiency of the two proteins. Inhibition of ferroptosis could reverse the weaken interaction of TFRC with THBS1 in vivo. TF can competitively bind TFRC with THBS1, and the binding of CD47 and THBS1 is also affected by ferroptosis and TFRC.

Multiple types of mechanical trauma (bone fracture, surgical damage, etc.) are among the most important factors that contribute to DVT. Damage to the vascular wall and surrounding tissue is the main initiator of the coagulation cascade. To simulate true clinical thrombosis, we chose a clamping method to generate FV damage and construct the

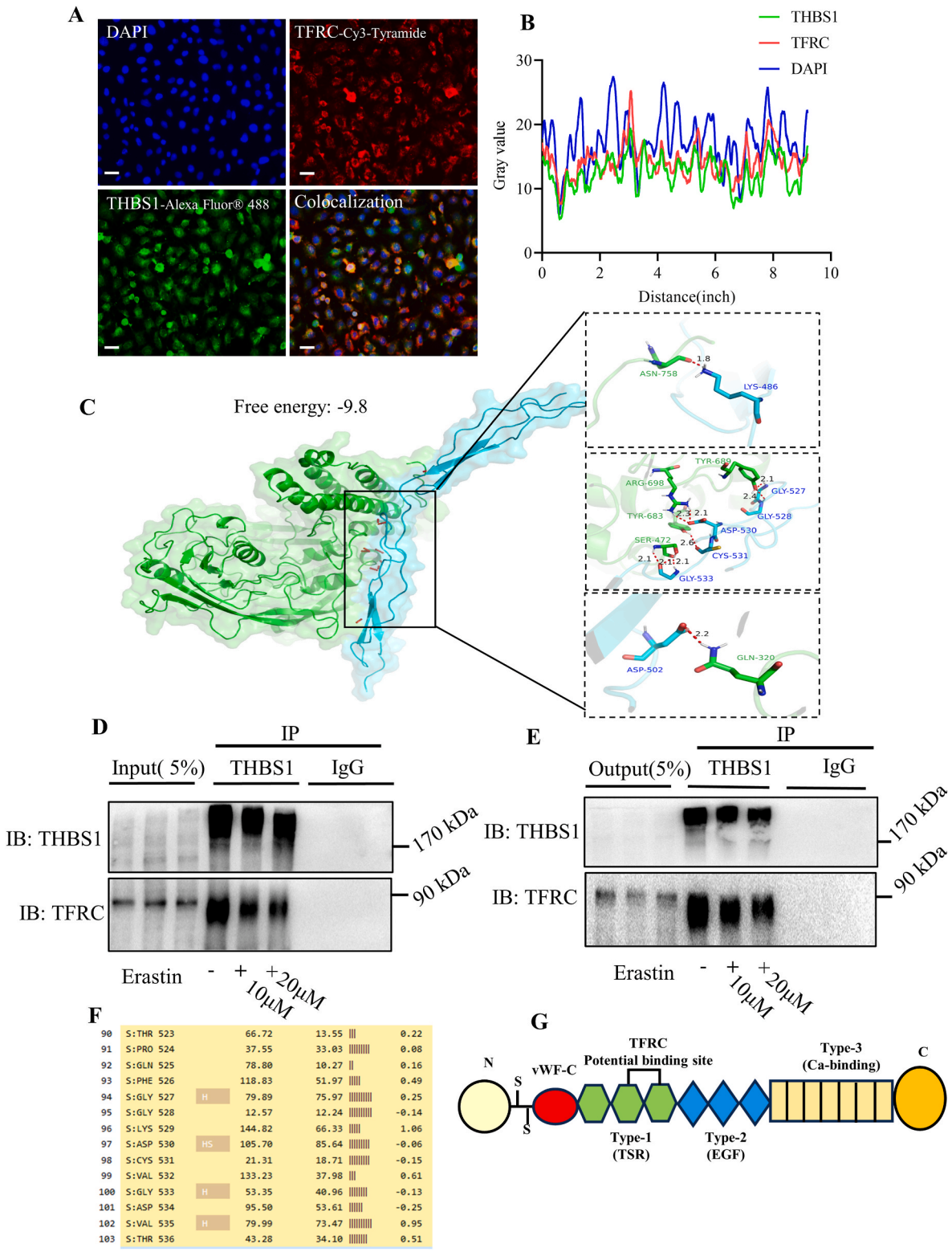

Fig. 9. TFRC interacts with THBS1, and this interaction is affected by ferroptosis. (A) Colocalization of TFRC and THBS1 immunofluorescence in normal HUVECs. DAPI was used to stain the cell nucleus (n = 3), and the scale bar indicates 200 μm. (B) Profile of immunofluorescence colocalization; coincident curves reflecting the level of colocalization. (C) Molecular docking of TFRC and THBS1. The green molecule represents TFRC, and the sky-blue molecule represents THBS1. GLN320, SER472, TYR683, TYR689, ARG698, and ASN758 of TFRC form hydrogen bonds with ASP502, GLY533, CYS533, ASP530, GLY528, GLY527, and LYS486 of THBS1. (D) (E) Co-IP experiments revealed the interaction between TFRC and THBS1 in the presence of various concentrations of erastin; n = 4. Input: positive control; IgG: negative control. (F) Co-IP results showing the interaction between TFRC and THBS1 in the presence of various concentrations of erastin; n = 3. Output: positive control of supernatant after coprecipitation; IgG: negative control. (G) Predicted TFRC binding domain in THBS1. The number of vertical lines reflects the possibility of binding. (H) The potential binding sites of TFRC in the structure of THBS1. (For interpretation of the references to color in this figure legend, the reader is referred to the Web version of this article.)

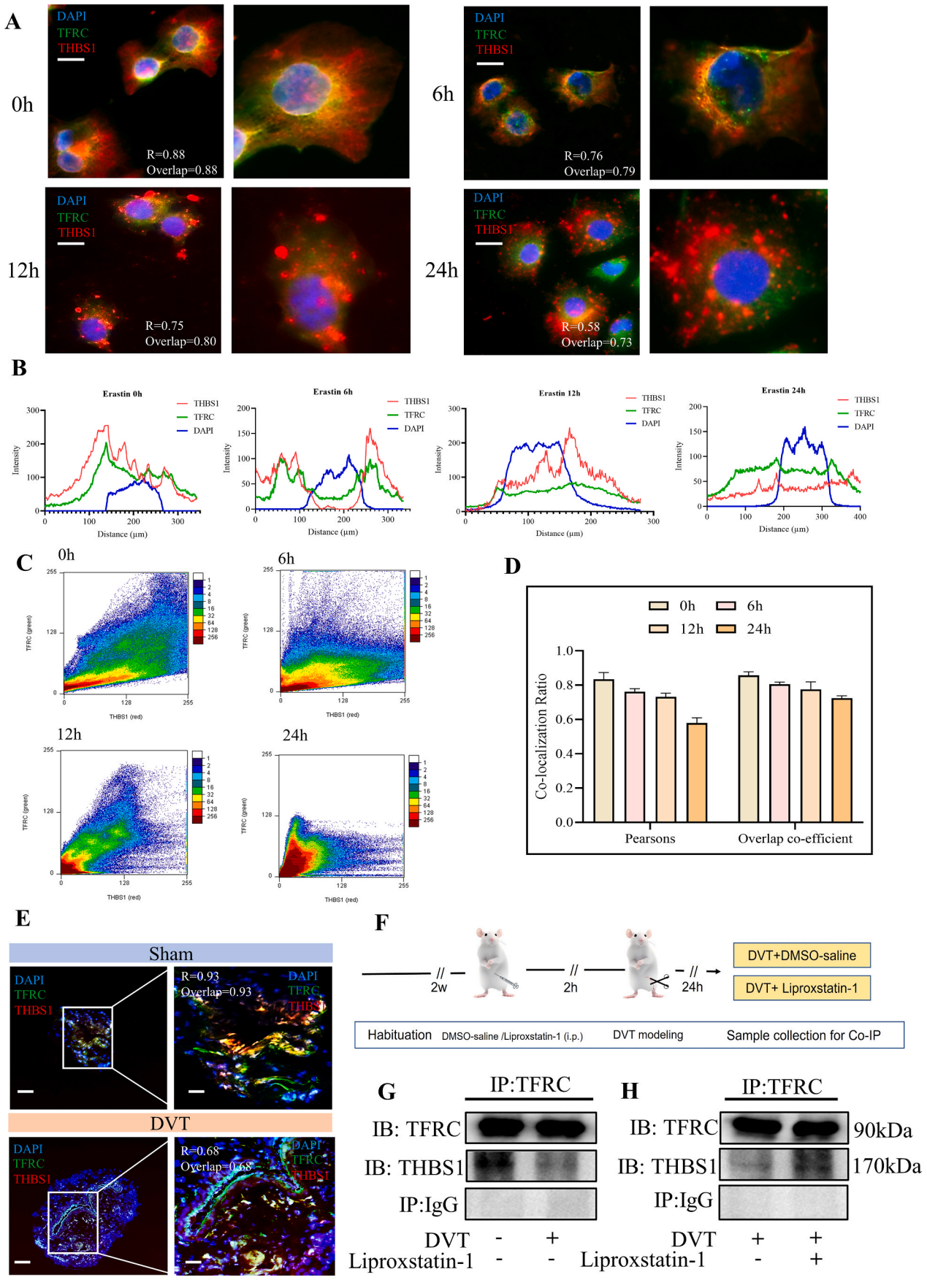

(caption on next page)

Fig. 10. Time course of erastin-induced ferroptosis and the effect on the interaction between TFRC and THBS1. (A) The effect of erastin on the interaction between TFRC and THBS1 was time-dependent (n = 4). The scale bar indicates 50 μm. (B) (C) The colocalization curves and scatter plots show the level of colocalization in the representative figure. (D) Colocalization ratio of THBS1 and TFRC after treatment with different concentrations of erastin for different durations; n = 4. (E) Immunofluorescence colocalization of TFRC and THBS1 in the sham and DVT groups (n = 3). All the samples were cross-sectioned, and the scale bar indicates 100 and 50 μm at low and high magnification, respectively. (F) Schematic representation of reverse ferroptosis in DVT models. (G) Co-IP experiment revealing the interaction between TFRC and THBS1 after DVT establishment, IgG: negative control. (H) Co-IP experiments revealed the interaction between TFRC and THBS1 after DVT establishment and in the presence or absence of liproxstatin-1; IgG: negative control.

thrombosis model. Multiple pathways participate in the thrombosis process. KEGG pathway enrichment analysis of the upregulated genes in the DVT/sham groups revealed that "complement/coagulation cascades", "regulation of the actin cytoskeleton", "neutrophil extracellular trap formation", "focal adhesion", "leukocyte transendothelial migration" and "ferroptosis" were the most important pathways. Complement/coagulation cascades and focal adhesion are classical thrombosis-related pathways [21]. The actin cytoskeleton can undergo rapid rearrangement, forming filopodia and lamellipodia while platelets spread; this process is also a prerequisite for normal platelet production and function [22,23]. Additionally, increased neutrophil extracellular trap formation can promote thrombosis [24]. The abovementioned roles of these pathways in thrombosis have been widely illustrated by previous studies. We also noticed that the "cell growth and death" pathway was enriched. Here, in this study, we focused mainly on the relationship between cell death and thrombosis. Vascular cells in thrombosis can undergo various types of cell death, including necroptosis and apoptosis. In 2004, Durand et al. reported that the in vivo induction of endothelial cell apoptosis leads to both vessel thrombosis and endothelial denudation [25]. Necroptosis plays pivotal roles in platelet prothrombotic responses and contributes to clot formation [26,27]. Notably, in this study, ferroptosis was the 14th pathway among the top 30 pathways identified via KEGG analysis (Figure B). The results indicated that ferroptosis was the most highly enriched cell death pathway, and the ratio of genes related to ferroptosis was higher than that of genes related to necroptosis, apoptosis, autophagy and mitophagy (Figure C). As in other pathways, hypoxic conditions in injured femoral veins may be reflected by activation of the HIF1 signaling pathway, which may increase the accumulation of iron and promote ferroptosis [28]. These results indicate that ferroptosis is significantly related to the risk of thrombosis, but the underlying mechanism is still unclear. Therefore, we began scientific investigations to address this.

Through WGCNA, TFRC was identified as a hub protein, and it has been reported to participate in several hemorrhagic disorders, such as β-thalassemia; however, very few reports on the role of TFRC in hemostasis and thrombosis exist [29,30]. A previous study reported that TFRC could be used as a diagnostic biomarker of DVT because its expression is upregulated in plasma samples from DVT patients [11]; however, TFRC in plasma is considered a soluble TFR, which is a truncated form of tissue TFR1 and is not suitable for comparison [31]. Here, we focused on the role of TFRC, which is mainly located on the vascular endothelium and regulates the import of iron. In this study, iron accumulation was observed in injured venous tissues, while the level of serum iron in the DVT group was decreased. First, we hypothesized that this unequal iron distribution may be caused by the high expression of TFRC. TFRC encodes TFR1, which is a membrane protein that regulates iron intake, has affinity for transferrin bound to Fe^{3+} ions and is the most crucial method for importing iron [32,33]. The tissue iron level was reduced after the expression of TFRC was knocked down, which could explain the iron overload in tissues. However, knockdown of venous TFRC had little effect on the serum iron distribution in DVT rats. An earlier study demonstrated that endothelial cell TFRC plays a minor role in systemic iron uptake, which is consistent with our hypothesis [34]. Major surgical operations and various traumas to rats can decrease serum iron, which may be the principal reason for this phenomenon [35]. TFRC is one of the crucial proteins that participate in ferroptosis [36,37]. Many lines of evidence indicate that ferroptosis contributes to thrombogenesis. Erythrophagocytosis-triggered ferroptosis in endothelial cells promoted thrombogenesis and could be suppressed by an iron chelator (deferoxamine) [38]; furthermore, single factors that are involved in ferroptosis have their own procoagulant effects. For instance, ROS can mediate endothelial cell functions and affect the modification of coagulation factors [39,40]; venous GPX4 was downregulated after DVT modeling as a result of severe oxidative stress. GPX4 is the first protective enzyme for *anti*-ferroptosis, and its depletion and inactivation indicated ferroptosis [41,42]. Moreover, GPX4 deficiency was reported to cause multiorgan thrombus formation in mice [43]. Thus, the connection between ferroptosis and thrombosis is complicated, but the initial element is iron accumulation. It was previously reported that knockdown of TFRC could increase the resistance to erastin-induced cell death and that knockout of TFRC expression significantly alleviated iron accumulation and inhibited ferroptosis [44]. The results indicate that the reduction in iron import caused by TFRC knockdown is implicated in ferroptosis. Here, we chose the AAV2/9 serotype as the vector to knock down TFRC. Different serotypes of AAV determine the transduction efficiency in different types of cells. AAV2 showed a markedly low level of endothelial cell transduction, but using AAV2/9 can result in successful transfection in arteries [45–47]. Blocking the blood supply of target vessels after AAV injection is a classic method to improve specific transduction efficiency, especially when selecting vectors with broad-spectrum promoters [48]. We further found TFRC knockdown upregulated the expression of GPX4 under ferroptosis in venous tissues.

Overall, TFRC interference ameliorated thrombogenesis in veins with mechanical injury. This effect can be attributed to the anti-ferroptotic effect of TFRC knockdown on vascular cells. However, this conclusion is broad with too many redundant pathways involved, and we believe that TFRC can also directly participate in thrombosis events. Previous research suggested that THBS1 was highly expressed in veins with DVT and that its expression was interfered with by a ferroptosis inhibitor, indicating that THBS1 may be related to ferroptosis. THBS1 belongs to the extracellular matrix thrombin-sensitive protein (THBS) family, and it was first discovered in platelets and can form homologous trimers and bind to the cell surface receptors CD36 and CD47 to exert various biological effects [49]. High expression of THBS1 is closely related to cell death, including apoptosis and pyroptosis [50,51]. However, the mechanism of THBS1 in ferroptosis remains unclear. This study was the first to report that THBS1 responded to erastin-induced ferroptosis in HUVECs. Similar to the effects on rats, lentivirus-mediated silencing of TFRC in HUVECs not only increased ferroptotic defense but also affected THBS1 expression. The level of THBS1 in the extracellular space was opposite that in the intracellular space. These findings prompted us to examine the interaction between TFRC and THBS1, especially in terms of protein secretion and endocytosis through transmembrane proteins. The interactions of THBS1 with other proteins mainly occur in the extracellular matrix or near the plasma membrane [52,53]. TFRC interacts with THBS1 through the TSR-2～ TSR-3 domains, unless there is an intermediate protein. TFRC knockdown also increased THBS1 levels in the extracellular matrix (ECM), suggesting that this interaction can regulate the secretion of THBS1.

THBS1 is highly expressed and activated after injury, thus exerting multiple cellular functions. Extracellular THBS1 can undergo several processes, including uptake, proteolysis or retention within the ECM. In HUVECs, THBS1 was found to be located mainly on the cytomembrane in response to erastin treatment, but its retention in the ECM was not observed. We think this effect may be related to an increase in the

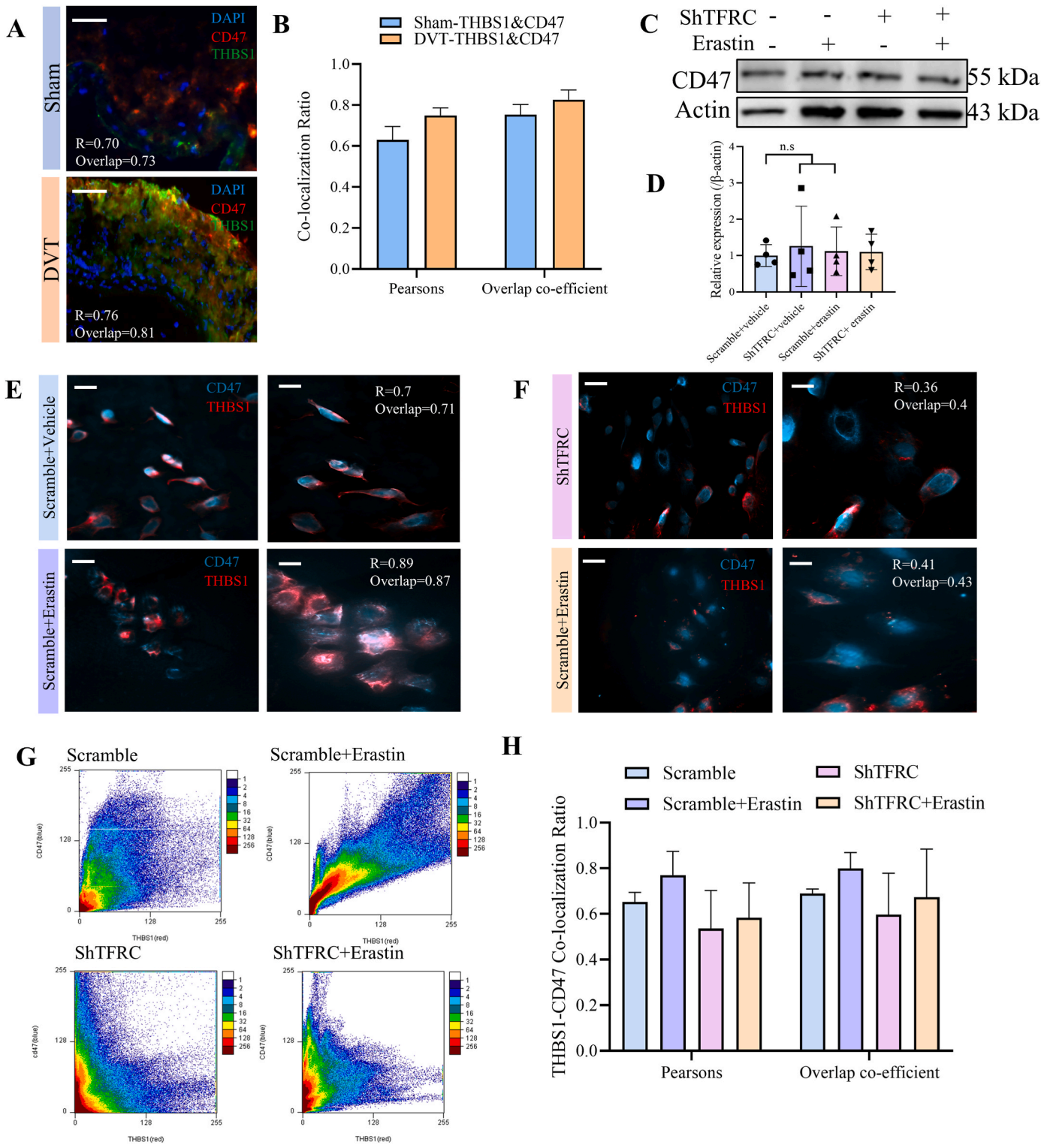

Fig. 11. Erastin-induced ferroptosis affects the binding of THBS1 to CD47. (A) Immunofluorescence colocalization of THBS1 and CD47 in venous tissues; n = 3. The scale bar indicates 50 μm. (B) The colocalization ratio of THBS1 and TFRC in the sham and DVT groups; n = 3. (C) Western blotting (n = 4) was used to determine the expression of CD47 (~55 kDa) in scramble-or shTFRC-transfected HUVECs. β-Actin (~43 kDa) was used as a loading control. (D) Quantification of the data in Fig. 11C. The protein levels were normalized to the actin level (n = 4); the values are expressed as the mean ± SD of replicates, and "n.s" ($P < 0.05$) indicates a non-significant difference between two groups according to the Mann−Whitney *U* test (E) Erastin-induced ferroptosis affects the colocalization of THBS1 and CD47. The scale bar indicates 100 μm and 50 μm at low and high magnification, respectively, n = 3. (F) TFRC knockdown affected the colocalization of THBS1 and CD47; n = 3. The scale bar indicates 100 μm and 50 μm at low and high magnification, respectively. (G) The scatter plots show the level of colocalization in the representative figure. (H) The visualized colocalization ratio of THBS1 and CD47 in HUVECs in the four groups; n = 3.

binding of THBS1 to other receptors based on the following evidence. On the one hand, a reduction in the interaction between THBS1 and TFRC was observed in injured veins and ferroptotic HUVECs; thus, THBS1 may eliminate a portion of TFRC and bind to other receptors. The extracellular THBS1 concentration was increased in TFRC-knockdown HUVECs (nonferroptotic conditions), but the intracellular THBS1 level was decreased, indicating that the uptake of THBS1 through receptors is limited under normal conditions. On the other hand, when ferroptosis occurs in HUVECs, the retention of THBS1 in the ECM decreases, and the interaction between THBS1 and CD47 increases. Moreover, a previous study revealed that activation of CD47 by THBS1 can stimulate ROS production and promote vascular dysfunction by promoting oxidative stress [54]. Moreover, as a bridging molecule that participates in hemostasis [55], THBS1 was observed to be located in the endothelial cytomembrane after erastin treatment, which could indicate the promotion of adhesion in response to ferroptosis. One of the ligands of THBS1 is the molecule CD36 [56]. This interaction occurs mainly between thrombospondin-1 TSR domains and the CLESH domain of CD36 [57], which might be affected by the weak interaction between TFRC and THBS1 during ferroptosis. These phenomena have far-reaching consequences for hypercoagulability and thrombogenesis. vWF is an important glycoprotein associated with hemostasis; it is sensitive to endothelial injury and acts as a linker at sites of vascular injury for platelet adhesion [58]. The extracellular vWF concentration was increased in ferroptotic HUVECs, while the extracellular THBS1 concentration was decreased; the latter has been indicated to control the multimer size of vWF and negatively regulates thrombus growth [59]. In addition, the interactions between THBS1 and CD47 and between THBS1 and CD36 can contribute to thrombus formation [60,61].

What could cause the interaction between TFRC and THBS1 to weaken during ferroptosis? On the surface of a target cell, transferrin is bound to TFRC, and the resulting TFRC complex is endocytosed into endosomes. Natural ligands with high affinity can competitively bind to the receptors of other proteins, such as TFRC and transferrin [62]. This study showed that exogenous supplementation with transferrin could reduce the interaction between TFRC and THBS1, which proved our hypothesis.

In the present study, the role of TFRC and its interaction with THBS1 during thrombogenesis were demonstrated. Specific regulation of endothelial TFRC is an efficient approach for regulating venous thrombosis and has little effect on iron homeostasis throughout the entire periphery [34]. However, there are several limitations of this study. For example, endothelial-specific promoters were not chosen for AAV transduction, and the consequences of TFRC overexpression were not elucidated because TFRC was already highly expressed in our model. Finally, the role of THBS1 in thrombus formation is still unclear in the vascular biology field. THBS1 can originate at injury sites of the endothelium in addition to platelet. Platelet-derived THBS1 has different biological effects on thrombosis, while the role of endothelial cell-derived THBS1 on thrombosis is still unclear. Here we explored only the effect of endothelial cell-derived THBS1. This study provides a new mechanistic framework for understanding thrombosis after vascular injury and proposes that two proteins interact in the endothelial ferroptosis-coagulation cascade; these findings will support future clinical research. Targeted interference with TFRC and THBS1 (such as by specific inhibitors) could be an approach for the treatment and prevention of venous mechanical injury-induced DVT. Moreover, monitoring iron homeostasis is necessary to prevent anticoagulation in clinical practice.

Taken together, these findings indicate that the upregulated expression of TFRC causes iron accumulation in injured venous tissues and induces secondary ferroptosis, which promotes thrombogenesis. TFRC knockdown inhibited ferroptosis and alleviated thrombus formation; moreover, TFRC and THBS1 interacted with each other, and their interaction was decreased in HUVECs during ferroptosis, which affected thrombus formation. These two proteins could be linked proteins associated with iron intake, ferroptosis and coagulation cascades.

CRediT authorship contribution statement

Haotian Ma: Writing – original draft, Visualization, Methodology, Investigation, Formal analysis, Data curation. **Yongtao Huang:** Resources, Methodology, Data curation. **Wenrong Tian:** Validation, Investigation, Data curation. **Jincen Liu:** Software, Methodology, Investigation. **Xinyue Yan:** Investigation, Data curation. **Lei Ma:** Writing – review & editing, Validation. **Jianghua Lai:** Writing – review & editing, Supervision, Project administration, Funding acquisition, Conceptualization.

Declaration of competing interest

No conflicts of interest to disclose.

Data availability

Data will be made available on request.

Acknowledgments

We thank Dr. Zilong Li from The First Affiliated Hospital of Xi'an Jiao Tong University, Dr. Meng Wang from Ocean University of China and Dr. Jing Xiao from Xi'an Jiao Tong University for their technical assistance.

Appendix A. Supplementary data

Supplementary data to this article can be found online at https://doi.org/10.1016/j.redox.2024.103041.

References

[1] M. Franchini, G. Targher, M. Montagnana, G. Lippi, Iron and thrombosis, Ann. Hematol. 87 (2008) 167–173.
[2] N. Li, W.Y. Jiang, W. Wang, R. Xiong, X.J. Wu, Q. Geng, Ferroptosis and its emerging roles in cardiovascular diseases, Pharmacol. Res. 166 (2021) 105466.
[3] H. Ma, X. Yan, J. Liu, Y. Lu, Y. Feng, J. Lai, Secondary ferroptosis promotes thrombogenesis after venous injury in rats, Thromb. Res. (216) (2022) 59–73.
[4] S.M. Day, D. Duquaine, L.V. Mundada, R.G. Menon, B.V. Khan, S. Rajagopalan, W. P. Fay, Chronic iron administration increases vascular oxidative stress and accelerates arterial thrombosis, Circulation 107 (2003) 2601–2606.
[5] S. Yang, Y. Zheng, X. Hou, Lipoxin A4 restores oxidative stress-induced vascular endothelial cell injury and thrombosis-related factor expression by its receptor-mediated activation of Nrf2-HO-1 axis, Cell. Signal. (60) (2019) 146–153.
[6] F.S. Türker, A. Malbora, M. Erisir, Oxidative status and antioxidant enzyme levels in deep venous thrombosis patients, Am J Cardiovasc Dis (11) (2021) 176–183.
[7] J. Yang, X. Zhou, X. Fan, M. Xiao, D. Yang, B. Liang, M. Dai, L. Shan, J. Lu, Z. Lin, R. Liu, J. Liu, L. Wang, M. Zhong, Y. Jiang, X. Bai, mTORC1 promotes aging-related venous thrombosis in mice via elevation of platelet volume and activation, Blood 128 (2016) 615–624.
[8] C. Gutmann, R. Siow, A.M. Gwozdz, P. Saha, A. Smith, Reactive oxygen species in venous thrombosis, Int. J. Mol. Sci. 21 (6) (2020) 1918.
[9] D. Tang, G. Kroemer, Ferroptosis, Curr Biol. 30 (21) (2020) R1292–r1297.
[10] K.T. Sawicki, A. De-Jesus, H. Ardehali, Iron metabolism in cardiovascular disease: physiology, mechanisms, and therapeutic targets, Circ. Res. (132) (2023) 379–396.
[11] A.A. Memon, K. Sundquist, M. PirouziFard, J.L. Elf, K. Strandberg, P.J. Svensson, J. Sundquist, B. Zöller, Identification of novel diagnostic biomarkers for deep venous thrombosis, Br. J. Haematol. 181 (3) (2018) 378–385.
[12] D. Wang, W. Liang, D. Huo, H. Wang, Y. Wang, C. Cong, C. Zhang, S. Yan, M. Gao, X. Su, X. Tan, W. Zhang, L. Han, D. Zhang, H. Feng, SPY1 inhibits neuronal ferroptosis in amyotrophic lateral sclerosis by reducing lipid peroxidation through regulation of GCH1 and TFR1, Cell Death Differ. (30) (2023) 369–382.
[13] Y. Zhao, H. Zhang, J.G. Cui, J.X. Wang, M.S. Chen, H.R. Wang, X.N. Li, J.L. Li, Ferroptosis is critical for phthalates driving the blood-testis barrier dysfunction via targeting transferrin receptor, Redox Biol. 59 (2023) 102584.
[14] A. Aburima, M. Berger, B.E.J. Spurgeon, B.A. Webb, K.S. Wraith, M. Febbraio, A. W. Poole, K.M. Naseem, Thrombospondin-1 promotes hemostasis through modulation of cAMP signaling in blood platelets, Blood 137 (2021) 678–689.
[15] S.S. Pierangeli, S.W. Liu, G. Anderson, J.H. Barker, E.N. Harris, Thrombogenic properties of murine anti-cardiolipin antibodies induced by beta 2 glycoprotein 1 and human immunoglobulin G antiphospholipid antibodies, Circulation (94) (1996) 1746–1751.

[16] M.A. Yerdel, B. Gunson, D. Mirza, K. Karayalçin, S. Olliff, J. Buckels, D. Mayer, P. McMaster, J. Pirenne, Portal vein thrombosis in adults undergoing liver transplantation: risk factors, screening, management, and outcome, Transplantation 69 (2000) 1873–1881.
[17] D. An, Q. Zeng, P. Zhang, Z. Ma, H. Zhang, Z. Liu, J. Li, H. Ren, D. Xu, Alpha-ketoglutarate ameliorates pressure overload-induced chronic cardiac dysfunction in mice, Redox Biol. 46 (2021) 102088.
[18] O.G. Lyublinskaya, J.S. Ivanova, N.A. Pugovkina, I.V. Kozhukharova, Z. V. Kovaleva, A.N. Shatrova, N.D. Aksenov, V.V. Zenin, Y.A. Kaulin, I.A. Gamaley, N.N. Nikolsky, Redox environment in stem and differentiated cells: a quantitative approach, Redox Biol. 12 (2017) 758–769.
[19] Y. Xu, F. Fang, S. Miriyala, P.A. Crooks, T.D. Oberley, L. Chaiswing, T. Noel, A. K. Holley, Y. Zhao, K.K. Kiningham, D.K. Clair, W.H. Clair, KEAP1 is a redox sensitive target that arbitrates the opposing radiosensitive effects of parthenolide in normal and cancer cells, Cancer Res. 73 (2013) 4406–4417.
[20] R.A. Swerlick, K.H. Lee, T.M. Wick, T.J. Lawley, Human dermal microvascular endothelial but not human umbilical vein endothelial cells express CD36 in vivo and in vitro, J. Immunol. 148 (1992) 78–83.
[21] G.F. Guidetti, M. Torti, I. Canobbio, Focal adhesion kinases in platelet function and thrombosis, Arterioscler. Thromb. Vasc. Biol. 39 (5) (2019) 857–868.
[22] Y. Schurr, A. Sperr, J. Volz, S. Beck, L. Reil, C. Kusch, P. Eiring, S. Bryson, M. Sauer, B. Nieswandt, L. Machesky, M. Bender, Platelet lamellipodium formation is not required for thrombus formation and stability, Blood 134 (25) (2019) 2318–2329.
[23] S. Stritt, S. Beck, I.C. Becker, T. Vögtle, M. Hakala, K.G. Heinze, X. Du, M. Bender, A. Braun, P. Lappalainen, B. Nieswandt, Twinfilin 2a regulates platelet reactivity and turnover in mice, Blood 130 (15) (2017) 1746–1756.
[24] O. Wolach, R.S. Sellar, K. Martinod, D. Cherpokova, M. McConkey, R.J. Chappell, A.J. Silver, D. Adams, C.A. Castellano, R.K. Schneider, R.F. Padera, D.J. DeAngelo, M. Wadleigh, D.P. Steensma, I. Galinsky, R.M. Stone, G. Genovese, S.A. McCarroll, B. Iliadou, C. Hultman, D. Neuberg, A. Mullally, D.D. Wagner, B.L. Ebert, Increased neutrophil extracellular trap formation promotes thrombosis in myeloproliferative neoplasms, Sci. Transl. Med. 10 (436) (2018) eaan8292.
[25] E. Durand, A. Scoazec, A. Lafont, J. Boddaert, A. Al Hajzen, F. Addad, M. Mirshahi, M. Desnos, A. Tedgui, Z. Mallat, In vivo induction of endothelial apoptosis leads to vessel thrombosis and endothelial denudation: a clue to the understanding of the mechanisms of thrombotic plaque erosion, Circulation 109 (21) (2004) 2503–2506.
[26] M. Ekhlak, P.P. Kulkarni, V. Singh, S.N. Chaurasia, S.K. Mohapatra, R.N. Chaurasia, D. Dash, Necroptosis executioner MLKL plays pivotal roles in agonist-induced platelet prothrombotic responses and lytic cell death in a temporal order, Cell Death Differ. 30 (8) (2023) 1886–1899.
[27] D. Nakazawa, J. Desai, S. Steiger, S. Müller, S.K. Devarapu, S.R. Mulay, T. Iwakura, H.J. Anders, Activated platelets induce MLKL-driven neutrophil necroptosis and release of neutrophil extracellular traps in venous thrombosis, Cell Death Dis. 28 (4) (2018) 6.
[28] L. Tacchini, E. Gammella, C. De Ponti, S. Recalcati, G. Cairo, Role of HIF-1 and NF-kappaB transcription factors in the modulation of transferrin receptor by inflammatory and anti-inflammatory signals, J. Biol. Chem. 283 (30) (2008) 20674–20686.
[29] X. Xiao, G. Moschetta, Y. Xu, A.L. Fisher, V.M. Alfaro-Magallanes, S. Dev, C. Y. Wang, J.L. Babitt, Regulation of iron homeostasis by hepatocyte TfR1 requires HFE and contributes to hepcidin suppression in β-thalassemia, Blood 141 (2023) 422–432.
[30] O. Weizer-Stern, K. Adamsky, N. Amariglio, E. Rachmilewitz, L. Breda, S. Rivella, G. Rechavi, mRNA expression of iron regulatory genes in beta-thalassemia intermedia and beta-thalassemia major mouse models, Am. J. Hematol. (81) (2006) 479–483.
[31] Y.J. Shih, R.D. Baynes, B.G. Hudson, C.H. Flowers, B.S. Skikne, J.D. Cook, Serum transferrin receptor is a truncated form of tissue receptor, J. Biol. Chem. (265) (1990) 19077–19081.
[32] H. Kawabata, Transferrin and transferrin receptors update, Free Radic. Biol. Med. (133) (2019) 46–54.
[33] M. Chen, Y. Zhang, K. Jiang, W. Wang, H. Feng, R. Zhen, C. Moo, Z. Zhang, J. Shi, C. Chen, Grab regulates transferrin receptor recycling and iron uptake in developing erythroblasts, Blood 140 (2022) 1145–1155.
[34] A.L. Fisher, C.Y. Wang, Y. Xu, K. Joachim, X. Xiao, S. Phillips, G.A. Moschetta, V. M. Alfaro-Magallanes, J.L. Babitt, Functional role of endothelial transferrin receptor 1 in iron sensing and homeostasis, Am. J. Hematol. (97) (2022) 1548–1559.
[35] L.N. An, Y. Yue, W.Z. Guo, Y.L. Miao, W.D. Mi, H. Zhang, Z.L. Lei, S.J. Han, L. Dong, Surgical trauma induces iron accumulation and oxidative stress in a rodent model of postoperative cognitive dysfunction, Biol. Trace Elem. Res. (151) (2013) 277–283.
[36] H. Feng, K. Schorpp, J. Jin, C.E. Yozwiak, B.G. Hoffstrom, A.M. Decker, P. Rajbhandari, M.E. Stokes, H.G. Bender, J.M. Csuka, P.S. Upadhyayula, P. Canoll, K. Uchida, R.K. Soni, K. Hadian, B.R. Stockwell, Transferrin receptor is a specific ferroptosis marker, Cell Rep. (30) (2020) 3411–3423.e7.
[37] L. Yi, Y. Hu, Z. Wu, Y. Li, M. Kong, Z.J. Kang, B.J. Zuoyuan, Z.C. Yang, TFRC upregulation promotes ferroptosis in CVB3 infection via nucleus recruitment of Sp1, Cell Death Dis. (13) (2022) 592.
[38] Z. Li, M. Yan, Z. Wang, Y. An, X.Y. Wei, T.T. Li, M.H. Xu, Y.S. Xia, L.Q. Wang, C. Y. Gao, Ferroptosis of Endothelial Cells Triggered by Erythrophagocytosis Contributes to Thrombogenesis in Uremia, Thromb Haemost., 2023.
[39] P. Golino, M. Ragni, P. Cirillo, V.E. Avvedimento, A. Feliciello, N. Esposito, A. Scognamiglio, B. Trimarco, G. Iaccarino, M. Condorelli, M. Chiariello, G. Ambrosio, Effects of tissue factor induced by oxygen free radicals on coronary flow during reperfusion, Nat. Med. (2) (1996) 35–40.
[40] W. Zhang, J. Wang, Z. Xie, H.M. Zou, Q.Q. Chen, L. Xu, L. Hu, N. Fang, J. Xu, J. Zhou, J. Liu, H.T. Ran, Z.G. Wang, Y. Zhang, D.J. Guo, Antithrombotic therapy by regulating the ROS-mediated thrombosis microenvironment and specific nonpharmaceutical thrombolysis using Prussian blue nanodroplets, Small 18 (2022) e2106252.
[41] B.R. Stockwell, J.P. Friedmann Angeli, H. Bayir, A.I. Bush, M. Conrad, S.J. Dixon, S. Fulda, S. Gascón, S.K. Hatzios, V.E. Kagan, K. Noel, X. Jiang, A. Linkermann, M. E. Murphy, M. Overholtzer, A. Oyagi, G.C. Pagnussat, J. Park, Q. Ran, C. S. Rosenfeld, K. Salnikow, D. Tang, F.M. Torti, S.V. Torti, S. Toyokuni, K. A. Woerpel, D. D. Zhang Ferroptosis, A regulated cell death nexus linking metabolism, Redox biology, and disease, Cell (171) (2017) 273–285.
[42] K. Bersuker, J.M. Hendricks, Z. Li, L. Magtanong, B. Ford, P.H. Tang, M.A. Roberts, B.Q. Tong, T.J. Maimone, R. Zoncu, M.C. Bassik z, D.K. Nomura, S.J. Dixon, J. A. Olzmann, The CoQ oxidoreductase FSP1 acts parallel to GPX4 to inhibit ferroptosis, Nature (575) (2019) 688–692.
[43] M. Wortmann, M. Schneider, J. Pircher, J. Hellfritsch, M. Aichler, N. Vegi, P. Kölle, P. Kuhlencordt, A. Walch, U. Pohl, G.W. Bornkamm, M. Conrad, H. Beck, Combined deficiency in glutathione peroxidase 4 and vitamin E causes multiorgan thrombus formation and early death in mice, Circ. Res. 113 (2013) 408–417.
[44] S. Lee, N. Hwang, B.G. Seok, S. Lee, S.J. Lee, S.W. Chung, Autophagy mediates an amplification loop during ferroptosis, Cell Death Dis. (14) (2023) 464.
[45] K. Pajusola, M. Gruchala, H. Joch, T.F. Lüscher, S.Y. Herttuala, H. Büeler, Cell-type-specific characteristics modulate the transduction efficiency of adeno-associated virus type 2 and restrain infection of endothelial cells, J. Virol. (76) (2002) 11530–11540.
[46] S. Wen, S. Graf, P.G. Massey, D.A. Dichek, Improved vascular gene transfer with a helper-dependent adenoviral vector, Circulation (110) (2004) 1484–1491.
[47] D. Pankajakshan, T.O. Makinde, R. Gaurav, M.D. Core, G. Hatzoudis, I. Pipinos, D. K. Agrawal, Successful transfection of genes using AAV-2/9 vector in swine coronary and peripheral arteries, J. Surg. Res. 175 (2012) 169–175.
[48] D.S. Chang, H. Su, G.L. Tang, L.S. Brevetti, R. Sarkar, R. Wang, Y.W. Kan, L. M. Messina, Adeno-associated viral vector-mediated gene transfer of VEGF normalizes skeletal muscle oxygen tension and induces arteriogenesis in ischemic rat hindlimb, Mol. Ther. (7) (2003) 44–51.
[49] S. Kaur, S.M. Bronson, D. Pal-Nath, T.W. Miller, D.R. Soto-Pantoja, D.D. Roberts, Functions of thrombospondin-1 in the tumor microenvironment, Int. J. Mol. Sci. (22) (2021) 4570.
[50] Y. Wu, H. Xiao, J. Pi, H. Zhang, A. Pan, Y.J. Pu, Z.H. Liang, J. Shen, J.P. Du, The circular RNA aplacirc_13267 upregulates duck granulosa cell apoptosis by the apla-miR-1-13/THBS1 signaling pathway, J. Cell. Physiol. (235) (2020) 5750–5763.
[51] J. Sun, X. Ge, Y. Wang, L. Niu, L.J. Tang, S.M. Pan, USF2 knockdown downregulates THBS1 to inhibit the TGF-β signaling pathway and reduce pyroptosis in sepsis-induced acute kidney injury, Pharmacol. Res. 176 (2022) 105962.
[52] A. Resovi, D. Pinessi, G. Chiorino, G. Taraboletti, Current understanding of the thrombospondin-1 interactome, Matrix Biol. (37) (2014) 83–91.
[53] K. Tan, M. Duquette, J.H. Liu, K. Shanmugasundaram, A. Joachimiak, J. T. Gallagher, A.C. Rigby, J.H. Wang, J. Lawler, Heparin-induced cis- and trans-dimerization modes of the thrombospondin-1 N-terminal domain, J. Biol. Chem. (283) (2008) 3932–3941.
[54] G. Csányi, M. Yao, A.I. Rodríguez, I.A. Ghouleh, M. Sharifi-Sanjani, G. Frazziano, X. Huang, E.E. Kelley, J.S. Isenberg, P.J. Pagano, Thrombospondin-1 regulates blood flow via CD47 receptor–mediated activation of NADPH oxidase 1, Arterioscler. Thromb. Vasc. Biol. (32) (2012) 2966–2973.
[55] K. Seif, L. Alidzanovic, B. Tischler, N. Ibrahim, B. Zagrapan, S. Rauscher, M. Salzmann, L. Hell, L.M. Mauracher, U. Budde, J.A. Schmid, B. Jilma, I. Pabinger, A. Assinger, P. Starlinger, C. Brostjan, Neutrophil-mediated proteolysis of thrombospondin-1 promotes platelet adhesion and string formation, Thromb. Haemostasis (118) (2018) 2074–2085.
[56] L.Y. Chu, D.P. Ramakrishnan, R.L. Silverstein, Thrombospondin-1 modulates VEGF signaling via CD36 by recruiting SHP-1 to VEGFR2 complex in microvascular endothelial cells, Blood (122) (2013) 1822–1832.
[57] P.A. Klenotic, R.C. Page, W. Li, S. Misra, R.L. Silverstein, Molecular basis of antiangiogenic thrombospondin-1 type 1 repeat domain interactions with CD36, Arterioscler. Thromb. Vasc. Biol. (33) (2013) 1655–1662.
[58] H. Wang, D. Li, Y. Chen, Z.Q. Liu, Y.Q. Liu, X.Y. Meng, H.J. Fan, S.K. Hou, Shear-induced acquired von Willebrand syndrome: an accomplice of bleeding events in adults on extracorporeal membrane oxygenation support, Front Cardiovasc Med (10) (2023) 1159894.
[59] L. Xie, C.N. Chesterman, P.J. Hogg, Control of von Willebrand factor multimer size by thrombospondin-1, J. Exp. Med. 193 (12) (2001) 1341–1349.
[60] A. Jeanne, T. Sarazin, M. Charlé, C. Kawecki, A. Kauskot, T. Hedtke, C.E. H. Schmelzer, L. Martiny, P. Maurice, S. Dedieu, Towards the therapeutic use of thrombospondin 1/CD47 targeting TAX2 peptide as an antithrombotic agent, Arterioscler. Thromb. Vasc. Biol. (41) (2021) e1–e17.
[61] R. Nergiz-Unal, M.M. Lamers, R. Van Kruchten, J.J. Luiken, J.M.E.M. Cosemans, J. F.C. Glatz, M.J.E. Kuijpers, J.W.M. Heemskerk, Signaling role of CD36 in platelet activation and thrombus formation on immobilized thrombospondin or oxidized low-density lipoprotein, J. Thromb. Haemostasis (9) (2011) 1835–1846.
[62] X. Wu, H. Liu, D. Han, B. Peng, H. Zhang, L. Zhang, J.L. Li, J. Liu, C. Cui, S.B. Fang, M. Li, M. Ye, W.H. Tan, Elucidation and structural modeling of CD71 as a molecular target for cell-specific aptamer binding, J. Am. Chem. Soc. 141 (2019) 10760–10769.